

The decays $\Sigma^+ \rightarrow p\ell^+\ell^-$ within the standard model and beyond⁰

Arnab Roy,^{1,*} Jusak Tandean,^{2,†} and German Valencia^{1,‡}

¹School of Physics and Astronomy, Monash University,¹

Wellington Road, Clayton, Victoria 3800, Australia¹

²Institute of High Energy Physics, Chinese Academy of Sciences, Beijing 100049, China²

(Dated: May 13, 2024)

Abstract

Motivated by the LHCb measurement of the hyperon decay mode $\Sigma^+ \rightarrow p\mu^+\mu^-$ and prospects for improvement, we revisit the estimates for the rate and muon forward-backward asymmetry within the standard model and beyond. The standard model prediction has a fourfold ambiguity, and we suggest ways to resolve it with other measurements, including possible studies of $\Sigma^+ \rightarrow pe^+e^-$ in the BESIII and LHCb experiments. We use the recent BESIII measurements of $\Sigma^+ \rightarrow p\gamma$ and $\Sigma^+ \rightarrow N\pi$ to reduce the uncertainty in the long-distance contribution to $\Sigma^+ \rightarrow p\mu^+\mu^-$. Beyond the standard model, we consider a general effective Hamiltonian at low energy with ten operators whose Wilson coefficients parametrize the new physics. We derive expressions for the $\Sigma^+ \rightarrow p\mu^+\mu^-$ rate and the associated muon forward-backward asymmetry in terms of these coefficients. Finally, we implement the existing constraints from kaon decays, pointing out the extent to which this hyperon mode can constrain the directions in parameter space to which the kaons are not sensitive.³

May 2024
[hep-ph] [hep-ph]
arXiv:2404.15268v2
183
196
196
13 15 17
21 4 5
13 15 17
21 4 5
13 15 17
24
160
89 77 95

* arnab.roy1@monash.edu
† jtandean@yahoo.com
‡ german.valencia@monash.edu

The LHCb Collaboration published a new measurement of the rate of the rare hyperon decay mode $\Sigma^+ \rightarrow p\mu^+\mu^-$ in 2018 [1] and is expected to present an improved analysis with more data soon. In combination with the renewed interest in future hyperon and kaon experiments [2–7], this motivates us to revisit the theoretical status of this mode both within the standard model (SM) and beyond.

In the SM the decays $\Sigma^+ \rightarrow p\ell^+\ell^-$ with $\ell = e, \mu$ each receive short-distance (SD) and long-distance (LD) contributions. The former are known to be significantly smaller than the latter [8]. We take another look at the SD component for completeness, as previous calculations have partly relied on the value of a Wilson coefficient that predates the discovery of the top quark [9]. We update this number with the formalism of Ref. [10], arriving at a larger value than what has been quoted before, but the corresponding total SD amplitude is still substantially below its LD counterpart.

Although the LD contributions dominate the rate, they suffer from multiple uncertainties, which include a fourfold ambiguity in the prediction [8]. Addressing this is one of the goals of this paper. Critical input to this examination is the measurement of the rate of the radiative channel $\Sigma^+ \rightarrow p\gamma$, where there is a recent precise result from the BESIII experiment [11]. We employ this information, along with a new fit to the nonleptonic decays $\Sigma^+ \rightarrow p\pi^0$ and $\Sigma^+ \rightarrow n\pi^+$ prompted by other recent BESIII data [12, 13], to reduce the uncertainty in the LD form-factors that derives from experimental input. The fourfold ambiguity in the SM estimation remains, and we propose possible measurements to resolve or alleviate this issue. The theoretical uncertainty in the LD calculation is partially quantified by considering extraction of the form factors in relativistic baryon chiral perturbation theory and in its heavy-baryon formulation.

After the complete SM treatment of $\Sigma^+ \rightarrow p\ell^+\ell^-$, we predict in the $\ell = \mu$ case the rate, the muon forward-backward asymmetry, the dimuon spectrum, and the additional observable f_L in the angular distribution, as well as the $\ell = e$ rate. The results are presented for the four solutions of the form factors that can be used for comparison with future experimental analyses.

We also consider the constraints that the $\ell = \mu$ mode can place on new physics (NP) parametrized in terms of ten Wilson coefficients in the low-energy effective Hamiltonian and how they are complementary to those arising from kaon decay modes. Even though the restrictions from the kaon sector are much stronger when they exist, we identify the directions in parameter space to which the kaon measurements are blind and constrain them with the existing information on the $\Sigma^+ \rightarrow p\mu^+\mu^-$ rate.

The structure of the rest of the paper is as follows. In Secs. II and III we deal respectively with the SD and LD amplitudes for $\Sigma^+ \rightarrow p\ell^+\ell^-$ in the SM and in Sec. IV evaluate the corresponding rates and other observables. In Sec. V we look at the impact on $\Sigma^+ \rightarrow p\ell^+\ell^-$ of potential NP manifesting itself via ten low-energy effective $s \rightarrow d\ell^+\ell^-$ operators, focusing on the $\ell = \mu$ case.

In Sec. VI we address the effects of the NP on various kaon observables. In Sec. VII we discuss the complementarity of the hyperon and kaon sectors in probing the NP. We give our conclusions in Sec. VIII.

10
10
10

II. SM SHORT-DISTANCE CONTRIBUTIONS

7 10 27

In the SM, the SD transition $s \rightarrow d\ell^+\ell^-$ arises from Z -penguin, box, and photon-penguin diagrams [9, 10, 14], which involve internal up-type quarks and W -boson. At QCD renormalization scales of order 1 GeV, this is described by the effective Hamiltonian [10]

$$\mathcal{H}_{\text{eff}}^{\text{SM}} = \frac{G_F}{\sqrt{2}} V_{ud}^* V_{us} \left[(z_{7V} + \tau y_{7V}) O_{7V} + \tau y_{7A} O_{7A} + C_{7\gamma} O_{7\gamma} \right], \quad (1) 6$$

where G_F is the Fermi coupling constant, V_{kl} denotes an element of the Cabibbo-Kobayashi-Maskawa (CKM) matrix, z_{7V} , $y_{7V,7A}$, and $C_{7\gamma}$ are the Wilson coefficients, $\tau = -V_{td}^* V_{ts} / (V_{ud}^* V_{us})$,

$$\begin{aligned} O_{7V} &= 2 \bar{d} \gamma^\kappa P_L s \bar{\ell} \gamma_\kappa \ell, & O_{7A} &= 2 \bar{d} \gamma^\kappa P_L s \bar{\ell} \gamma_\kappa \gamma_5 \ell, \\ O_{7\gamma} &= \frac{e}{8\pi^2} \bar{d} \sigma^{\kappa\nu} (m_s P_R + m_d P_L) s F_{\kappa\nu}, & P_{L,R} &= \frac{1}{2} (1 \mp \gamma_5), \end{aligned} \quad (2) 168$$

with e being the proton's electric charge, $m_{d(s)}$ the $d(s)$ -quark mass, and $F_{\kappa\nu}$ the photon field-strength tensor. The total SD contribution to the amplitude for $\Sigma^+ \rightarrow p\ell^+\ell^-$ is then

$$\begin{aligned} \mathcal{M}_{\text{SM}}^{\text{SD}} &= \langle p\ell^+\ell^- | \mathcal{H}_{\text{eff}}^{\text{SM}} | \Sigma^+ \rangle \\ &= \frac{G_F V_{ud}^* V_{us}}{\sqrt{2}} \left\{ \langle p | \bar{d} \gamma^\kappa (1 - \gamma_5) s | \Sigma^+ \rangle \left[(z_{7V} + \tau y_{7V}) \bar{u}_\ell \gamma_\kappa v_{\bar{\ell}} + \tau y_{7A} \bar{u}_\ell \gamma_\kappa \gamma_5 v_{\bar{\ell}} \right] \right. \\ &\quad \left. - \frac{i\alpha_e C_{7\gamma} m_s}{2\pi q^2} \langle p | \bar{d} \sigma^{\nu\kappa} (1 + \gamma_5) s | \Sigma^+ \rangle q_\kappa \bar{u}_\ell \gamma_\nu v_{\bar{\ell}} \right\} \quad 17 \quad 21 \quad 26 \end{aligned} \quad (3) 14$$

where u_ℓ ($v_{\bar{\ell}}$) represents the Dirac spinor of the emitted (anti)lepton, $\alpha_e = e^2/(4\pi)$, terms linear in m_d have been dropped from the last line because $m_d \ll m_s$, and $q = P_\Sigma - P_p$ is the difference between the Σ^+ and proton momenta.

To examine the decay rate from $\mathcal{M}_{\text{SM}}^{\text{SD}}$ requires knowing the hadronic matrix elements in it. From the leading-order strong Lagrangian in chiral perturbation theory (χ PT), one derives [15]

$$\begin{aligned} \langle p | \bar{d} \gamma^\kappa s | \Sigma^+ \rangle &= -\bar{u}_p \gamma^\kappa u_\Sigma, \\ \langle p | \bar{d} \gamma^\kappa \gamma_5 s | \Sigma^+ \rangle &= (D - F) \left(\bar{u}_p \gamma^\kappa \gamma_5 u_\Sigma + \frac{m_\Sigma + m_p}{q^2 - m_{K^0}^2} q^\kappa \bar{u}_p \gamma_5 u_\Sigma \right) \end{aligned} \quad 17 \quad 21 \quad 26 \quad (4) 21 \quad 0$$

where $u_{p,\Sigma}$ ($m_{p,\Sigma}$) denote the Dirac spinors (masses) of the baryons, D and F are parameters which can be determined from the measurements on hyperon semileptonic decays [16], and m_{K^0}

is the neutral-kaon mass. For the tensor currents, one can express¹ [21]

$$\langle p | \bar{d} \sigma^{\kappa\nu} (1, \gamma_5) s | \Sigma^+ \rangle \varepsilon_\kappa^* q_\nu = c_\sigma \bar{u}_p \sigma^{\kappa\nu} (1, \gamma_5) u_\Sigma \varepsilon_\kappa^* q_\nu, \quad (5)$$

where ε stands for the polarization four-vector of an on-shell photon and c_σ is a constant. [23]

Numerically, we adopt the CKM parameters available from Ref. [17], the Wilson coefficients typically given in the literature, namely $z_{7V} = -0.046\alpha_e$, $y_{7V} = 0.73\alpha_e$, $y_{7A} = -0.68\alpha_e$ [10, 18], and $C_{7\gamma} = 0.72$ [19, 20],² and $m_s = 123$ MeV, all evaluated at a renormalization scale of 1 GeV, with $\alpha_e = \alpha_e(m_Z) = 1/127.95$ [17]. For the Σ^+ lifetime and hadron masses, we employ the ones supplied by Ref. [17]. We also have $c_\sigma = 0.3$ from a quark-model computation [21] and $D = 0.81 \pm 0.01$ and $F = 0.47 \pm 0.01$ from fitting to baryon semileptonic decay data [17]. [25]

From the foregoing, the SD amplitude induced by $O_{7\gamma}$ (O_{7V} and O_{7A}) alone yields the branching fractions $\mathcal{B}(\Sigma^+ \rightarrow pe^+e^-)_{SD} = 2.6 (0.25) \times 10^{-10}$ and $\mathcal{B}(\Sigma^+ \rightarrow p\mu^+\mu^-)_{SD} = 1.3 (1.1) \times 10^{-12}$. They change to $\mathcal{B}(\Sigma^+ \rightarrow pe^+e^-)_{SD} = 2.7 \times 10^{-10}$ and $\mathcal{B}(\Sigma^+ \rightarrow p\mu^+\mu^-)_{SD} = 6.5 \times 10^{-13}$ if O_{7V} and $O_{7V,7A}$ are present simultaneously, indicating partial cancellation among their contributions in the muon case. These numbers are 4 to 5 orders of magnitude smaller than their experimental counterparts [1, 17, 22, 23]. [26]

III. SM LONG-DISTANCE CONTRIBUTIONS

[7] [10] [27]

The SD contribution being relatively tiny, the dominant component of $\Sigma^+ \rightarrow pl^+\ell^-$ has been estimated to be the long-distance photon-mediated process $\Sigma^+ \rightarrow p\gamma^* \rightarrow pl^+\ell^-$. If the photon is on-shell, the amplitude is parametrized by two form factors [24], a and b , that can be partly determined via the radiative weak decay $\Sigma^+ \rightarrow p\gamma$. For the latter mode, the effective Lagrangian has the form [28]

$$\mathcal{L}_{\Sigma^+ \rightarrow p\gamma} = \frac{eG_F}{2} \bar{p}(a + \gamma_5 b) \sigma^{\kappa\nu} \Sigma^+ F_{\kappa\nu}, \quad (6)$$

implying a partial width Γ_γ and distribution $d\Gamma_\gamma/d(\cos\vartheta)$ given by [30]

$$\begin{aligned} \Gamma_\gamma &= \frac{e^2 G_F^2}{\pi} (|a|^2 + |b|^2) E_\gamma^3, \\ \frac{d\Gamma_\gamma}{d(\cos\vartheta)} &\sim 1 + \alpha_\gamma \cos\vartheta, \quad \alpha_\gamma = \frac{2 \operatorname{Re}(ab^*)}{|a|^2 + |b|^2}, \end{aligned} \quad (7)$$

where E_γ denotes the photon's energy in the rest frame of the Σ^+ and ϑ is the angle between its polarization and the proton's three-momentum in this frame [17]. [32]

¹ Although $\langle p | \bar{d} \sigma^{\kappa\nu} s | \Sigma^+ \rangle$ involves four form-factors which are functions of q^2 , after contracting it with $\varepsilon_\kappa^* q_\nu$, and imposing $\varepsilon \cdot q = 0$ only one combination of them remains at $q^2 = 0$, as Eq. (5) indicates. The matrix element of $\bar{d} \sigma^{\kappa\nu} \gamma_5 s$ is related to that of $\bar{d} \sigma^{\kappa\nu} s$ because of the identity $2i\sigma^{\kappa\nu}\gamma_5 = \epsilon^{\kappa\nu\varphi\varsigma}\sigma_{\varphi\varsigma}$. [39]

² This is nearly real, results mainly from $O_{7\gamma}$ mixing with $O_2 = \bar{d}\gamma^\nu P_L u \bar{u}\gamma_\nu P_L s$ under QCD renormalization [10], and is hugely enhanced relative to the value without QCD corrections, $C_{7\gamma} = (-7.1 - 2.5i) \times 10^{-4}$, which is dominated by the top contribution, the charm and up ones being four times smaller and negligible, respectively. [24]

When the photon is virtual, the amplitude for $\Sigma^+ \rightarrow p\gamma^*$ contains two additional form-factors [25, 26], c and d , and is expressible as [33]

$$\mathcal{M}(\Sigma^+ \rightarrow p\gamma^*) = -eG_F \bar{u}_p [i\sigma^{\kappa\nu} q_\kappa (a + \gamma_5 b) + (\gamma^\nu q^2 - q^\kappa q^\nu) (c + \gamma_5 d)] u_\Sigma \varepsilon_\nu^*, \quad (8)$$

where q stands for the photon's four-momentum. Its contribution to $\Sigma^+ \rightarrow p\ell^+\ell^-$ is then found [35] to be [35]

$$\mathcal{M}_{\text{SM}}^{\text{LD}} = e^2 G_F \left[\frac{-i}{q^2} \bar{u}_p (a + \gamma_5 b) \sigma^{\kappa\nu} q_\kappa u_\Sigma - \bar{u}_p \gamma^\nu (c + \gamma_5 d) u_\Sigma \right] \bar{u}_\ell \gamma_\nu v_\ell. \quad (9)$$

In general a , b , c , and d depend on q^2 and can be complex, and the first two are constrained at $q^2 = 0$ by the data in the real-photon case, to which we turn next. [37]

There is experimental information available on the branching fraction \mathcal{B}_γ of $\Sigma^+ \rightarrow p\gamma$ and its decay asymmetry parameter α_γ , mostly gathered decades ago [17]. Last year BESIII reported fresh data on these quantities [11]: [36]

$$\begin{aligned} \mathcal{B}_\gamma &= (0.996 \pm 0.021_{\text{stat}} \pm 0.018_{\text{syst}}) \times 10^{-3}, \\ \alpha_\gamma &= -0.652 \pm 0.056_{\text{stat}} \pm 0.020_{\text{syst}}. \end{aligned} \quad (10)$$

The former is less than the corresponding value of $(1.23 \pm 0.05) \times 10^{-3}$ from the Particle Data Group (PDG) [17] by 4.2 standard deviations and also has a better precision [11], whereas the α_γ finding is consistent with the prior measurements [27–30]. Accordingly, for numerical work, we may simply adopt the \mathcal{B}_γ number in Eq. (10), while for α_γ we can take the average of the BESIII and earlier results, which is $\alpha_\gamma = -0.694 \pm 0.047$. Putting together these choices with Eq. (7) and employing the hadron masses and Σ^+ lifetime from Ref. [17], we then arrive at the $q^2 = 0$ combinations [41]

$$\begin{aligned} |a(0)|^2 + |b(0)|^2 &= (13.48 \pm 0.19)^2 \text{ MeV}^2, \\ \text{Re}(a(0) b^*(0)) &= (-63.1 \pm 4.6) \text{ MeV}^2, \end{aligned} \quad (11)$$

having additionally used $e^2 = 4\pi\alpha_e(0)$, with $\alpha_e(0) = 1/137.036$ [17], in Γ_γ . The LHCb experiment may be able to measure \mathcal{B}_γ and α_γ as well as they have measured similar quantities in the b -baryon sector [31]. [45]

As elaborated in Ref. [8], to work out how a , b , c , and d depend on q^2 , first their imaginary parts can be computed by means of relativistic baryon χ PT with the aid of unitarity arguments, and among the main inputs are the empirical S-wave and P-wave amplitudes for the nonleptonic channels $\Sigma^+ \rightarrow p\pi^0, n\pi^+$. Subsequently, with the resulting $\text{Im}(a, b)$ evaluated at $q^2 = 0$, the real parts of a and b are approximated to be constant and fixed from the observed \mathcal{B}_γ and α_γ values of $\Sigma^+ \rightarrow p\gamma$, up to a fourfold ambiguity. For the real parts of c and d , which are still empirically inaccessible, they are estimated using the vector-meson-dominance approach. Since there are new relevant data on $\Sigma^+ \rightarrow p\pi^0, n\pi^+$ from BESIII [12, 13], this procedure needs to be updated.

Thus, writing the amplitude for $\Sigma^+ \rightarrow N\pi$ as $\mathcal{M}_{\Sigma^+ \rightarrow N\pi} = iG_F m_\pi^2 \bar{\mu}_N (A_{N\pi} \gamma_5 B_{N\pi}) u_\Sigma$ and neglecting the small phases of $A_{N\pi}$ and $B_{N\pi}$, we arrive at³ 195 204 107 63

$$\begin{aligned} A_{n\pi^+} &= 0.047 \pm 0.004, & B_{n\pi^+} &= 18.54 \pm 0.07, \\ A_{p\pi^0} &= -1.383 \pm 0.021, & B_{p\pi^0} &= 12.32 \pm 0.24. \end{aligned} \quad (12) \quad 46$$

With these, we obtain $\text{Im } a(0) = (2.857 \pm 0.046) \text{ MeV}$ and $\text{Im } b(0) = (-1.742 \pm 0.040) \text{ MeV}$, which with Eq. (11) lead to the four solutions collected in the upper half of Table I. Employing heavy-baryon χ PT instead yields $\text{Im } a(0) = (6.98 \pm 0.10) \text{ MeV}$ and $\text{Im } b(0) = (-0.43 \pm 0.03) \text{ MeV}$, and hence another four solutions placed in the lower half of Table I. In all of our figures we will distinguish between the solutions listed in this table with the color coding: blue for solution 1, yellow solution 2, green solution 3, and red solution 4.⁴⁶

It is interesting to mention that, as pointed out long ago [24], the parameter⁵⁴

$$\gamma_\gamma = \frac{|a(0)|^2 - |b(0)|^2}{|a(0)|^2 + |b(0)|^2} \quad (13) \quad 50$$

may be determined in a weak radiative hyperon decay if the linear polarization of the photon⁵⁵ and the spins of the initial and final baryons can all be detected. If so, γ_γ in $\Sigma^+ \rightarrow p\gamma$ could reduce the fourfold ambiguity to a twofold ambiguity. For the situation illustrated by Table I, from the top (bottom) half we get $\gamma_\gamma = 0.72 \pm 0.04$ for solutions 1 and 4 and $\gamma_\gamma = -0.66 \pm 0.04$ ⁵⁶

Re a (MeV)	Re b (MeV)	$10^8 \mathcal{B}_{\mu\mu}$	$10^8 \mathcal{B}_{\mu\mu}^{\text{Re}(c,d)=0}$	$10^5 \tilde{A}_{FB}$	$10^6 \mathcal{B}_{ee}$	$10^7 \mathcal{B}_{ee}^{M_{ee} \geq 100 \text{ MeV}}$
-12.15 ± 0.24	4.78 ± 0.42	2.7 ± 0.2	1.8 ± 0.1	-1.59 ± 0.04	7.6 ± 0.3	8.5 ± 0.4
-4.78 ± 0.42	12.15 ± 0.24	7.8 ± 0.3	5.8 ± 0.2	-0.32 ± 0.02	8.3 ± 0.3	13.5 ± 0.4
4.78 ± 0.42	-12.15 ± 0.24	4.2 ± 0.2	5.8 ± 0.2	0.91 ± 0.04	7.8 ± 0.3	9.9 ± 0.4
12.15 ± 0.24	-4.78 ± 0.42	1.2 ± 0.1	1.8 ± 0.1	4.55 ± 0.08	7.4 ± 0.3	6.9 ± 0.3
Re a (MeV)	Re b (MeV)	$10^8 \mathcal{B}_{\mu\mu}$	$10^8 \mathcal{B}_{\mu\mu}^{\text{Re}(c,d)=0}$	$10^5 \tilde{A}_{FB}$	$10^6 \mathcal{B}_{ee}$	$10^7 \mathcal{B}_{ee}^{M_{ee} \geq 100 \text{ MeV}}$
-9.74 ± 0.54	6.17 ± 0.74	3.7 ± 0.5	2.7 ± 0.3	-0.73 ± 0.06	7.9 ± 0.5	10.2 ± 0.8
-6.17 ± 0.74	9.74 ± 0.54	6.1 ± 0.5	4.5 ± 0.4	-0.29 ± 0.05	8.3 ± 0.6	12.6 ± 0.8
6.17 ± 0.74	-9.74 ± 0.54	3.2 ± 0.3	4.5 ± 0.4	1.49 ± 0.09	7.8 ± 0.6	9.7 ± 0.7
9.74 ± 0.54	-6.17 ± 0.74	1.9 ± 0.2	2.7 ± 0.3	3.2 ± 0.1	7.6 ± 0.5	8.3 ± 0.6

TABLE I. The four solutions for the real parts of the form factors a and b (columns 1-2) obtained in relativistic baryon χ PT (first four rows) and in its heavy-baryon formulation (last four rows) and the corresponding predictions in the SM for each case (columns 3-7). In the third and fourth columns $\mathcal{B}_{\mu\mu} \equiv \mathcal{B}(\Sigma^+ \rightarrow p\mu^+\mu^-)$ is from the complete SM amplitude and $\mathcal{B}_{\mu\mu}^{\text{Re}(c,d)=0}$ gets no contribution from the real parts of the form factors c and d . In the fifth column \tilde{A}_{FB} is the integrated muon forward-backward asymmetry. The last two columns exhibit $\mathcal{B}_{ee} \equiv \mathcal{B}(\Sigma^+ \rightarrow pe^+e^-)$ without and with a cut in the dielectron invariant mass.⁵³

³ We have used the branching fractions $\mathcal{B}(\Sigma^+ \rightarrow n\pi^+) = (48.31 \pm 0.30)\%$ and $\mathcal{B}(\Sigma^+ \rightarrow p\pi^0) = (51.57 \pm 0.30)\%$ from Ref. [17], based on measurements done over 40 years ago, as well as the decay asymmetry parameters $\alpha_\pi(\Sigma^+ \rightarrow p\pi^0) = -0.993 \pm 0.004$ and $\alpha_\pi(\Sigma^+ \rightarrow n\pi^+) = 0.052 \pm 0.004$ from averaging the respective recent BESIII findings on these observables [12, 13] and the corresponding earlier measurements [32–35].⁵⁰

for solutions 2 and 3 ($\gamma_\gamma = 0.58 \pm 0.10$ for solutions 1 and 4 and $\gamma_\gamma = -0.05 \pm 0.11$ for solutions 2 and 3). We see that just a measurement of the sign of γ_γ may suffice to decrease the ambiguity 56 to twofold. 56

It may be that resolving this ambiguity completely, as well as minimizing other uncertainties in 57 the LD contributions, will only be possible if they are addressed on the lattice. Initial exploratory 57 efforts along this direction have recently been undertaken, as detailed in Refs. [36, 37]. 57

IV. DECAY RATES AND OBSERVABLES

The different contributions to $\Sigma^+ \rightarrow p\ell^+\ell^-$ can be incorporated into the general expression 59 for the amplitude [38] 59

$$\mathcal{M} = [iq_\kappa \bar{u}_p(\tilde{A} + \gamma_5 \tilde{B})\sigma^{\nu\kappa}u_\Sigma - \bar{u}_p\gamma^\nu(\tilde{C} + \gamma_5 \tilde{D})u_\Sigma]\bar{u}_\ell\gamma_\nu v_{\bar{\ell}} + \bar{u}_p\gamma^\nu(\tilde{E} + \gamma_5 \tilde{F})u_\Sigma \bar{u}_\ell\gamma_\nu \gamma_5 v_{\bar{\ell}} + \bar{u}_p(\tilde{G} + \gamma_5 \tilde{H})u_\Sigma \bar{u}_\ell v_{\bar{\ell}} + \bar{u}_p(\tilde{J} + \gamma_5 \tilde{K})u_\Sigma \bar{u}_\ell \gamma_5 v_{\bar{\ell}}, \quad (14) 67$$

where $q = P_\Sigma - P_p = P_+ + P_-$, with P_\pm denoting the four-momenta of ℓ^\pm , and $\tilde{A}, \tilde{B}, \dots, \tilde{K}$ are 61 generally complex quantities, some of which depend on q^2 and which may contain both SM and 61 NP contributions. The formula for the rate derived from \mathcal{M} can be found in Ref. [38] and hence 61 will not be reproduced here. 61

From Secs. II and III, the SD and LD amplitudes in the SM yield 62

$$\begin{aligned} \tilde{A} &= \frac{G_F}{q^2} \left(a e^2 - \frac{\lambda_u^* c_\sigma C_{7\gamma} e^2 m_s}{\sqrt{2} 8\pi^2} \right), & \tilde{B} &= \frac{G_F}{q^2} \left(b e^2 \frac{c_\sigma C_{7\gamma} e^2 m_s}{\sqrt{2} 13 8\pi^2} \right), & 21 & 26 & 21 & 169 \\ \tilde{C} &= G_F \left(c e^2 + \frac{\lambda_u^* z_{7V} - \lambda_t^* y_{7V}}{\sqrt{2}} \right), & \tilde{D} &= G_F \left(d e^2 \frac{\lambda_u^* z_{7V} - \lambda_t^* y_{7V}}{\sqrt{2}} \right), & 7 & 21 & 26 \\ \tilde{E} &= \frac{G_F}{\sqrt{2}} \lambda_t^* y_{7A}, & \tilde{F} &= \frac{D - F}{\sqrt{2}} G_F \lambda_t^* y_{7A}, & 63 & 146 & 189 \\ \tilde{K} &= \sqrt{2}(D - F)G_F \lambda_t^* y_{7A} m_e \frac{m_\Sigma + m_p}{q^2 - m_{K^0}^2} \frac{7}{63} \frac{21}{102} \frac{26}{113} & & & & & & (15) 50 \end{aligned}$$

where $\lambda_q^* = V_{qd}^* V_{qs}$. These lead to the SM predictions for $\mathcal{B}_{\mu\mu} = \mathcal{B}(\Sigma^+ \rightarrow p\mu^+\mu^-)$ and 64 other observables collected in the third through fourth columns of Table I, where the quoted 64 errors have been translated from the ranges of $\text{Re}(a, b)$ in columns 1-2 and of the corresponding 64 $\text{Im}(a(0), b(0))$ computed in the preceding section. Parametric uncertainty in other quantities 64 entering these predictions is much smaller, and so we ignore it. 64

Implicit in the results listed in Table I is the presence of hadronic model dependence which 66 occurs in the treatment of the real parts of c and d , discussed in Ref. [8]. One can get an indication 66 about the extent of this model dependence in, for instance, the $\Sigma^+ \rightarrow p\mu^+\mu^-$ branching fraction 66 by comparing the entries in the third and fourth columns of this table. It is also instructive to 66 estimate the theoretical uncertainty arising from the extraction of the imaginary parts of the 66

form factors at $q^2 = 0$ by comparing the results derived with relativistic baryon χ PT and with its heavy-baryon formulation. The range of predictions obtained by interpolating between these two is displayed in Fig. 1.

The PDG [17] currently quotes $\mathcal{B}(\Sigma^+ \rightarrow p\mu^+\mu^-)_{\text{PDG}} = (2.4^{+1.7}_{-1.3}) \times 10^{-8}$, based on the findings of the HyperCP [23] and LHCb [1] experiments. It would seem, in view of Table I and Fig. 1, to be in conflict with the predictions of solution 2, but one of them, $\mathcal{B}_{\mu\mu} = (6.1 \pm 0.5) \times 10^{-8}$

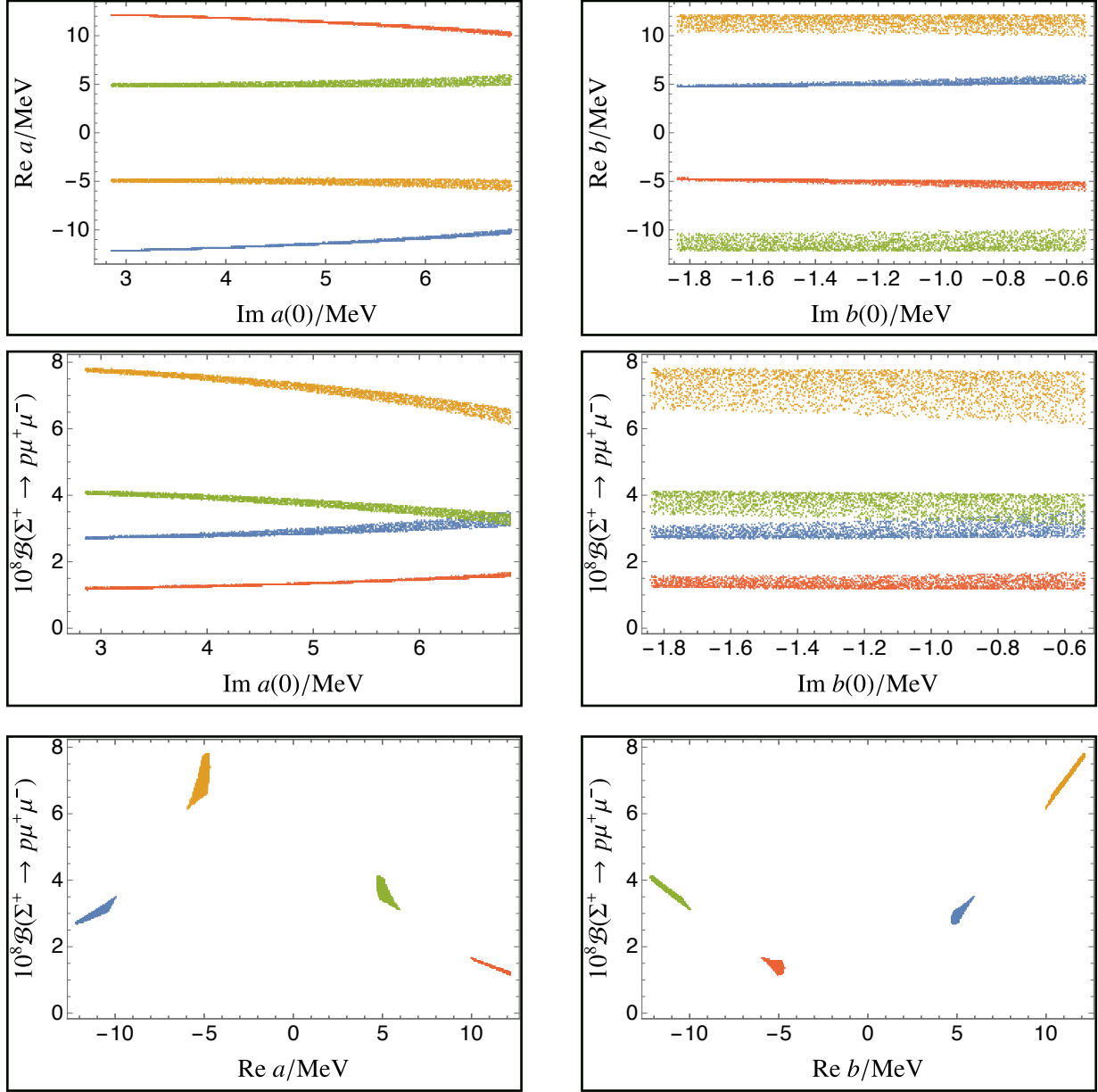


FIG. 1. Variation in the real parts of the form factors a and b (top row) and in the resulting branching fraction $\mathcal{B}(\Sigma^+ \rightarrow p\mu^+\mu^-)$ (middle row) as $\text{Im } a(0)$ and $\text{Im } b(0)$ are allowed to vary between the values determined with relativistic baryon χ PT and with its heavy-baryon formulation. The bottom plots show the corresponding correlations between $\mathcal{B}(\Sigma^+ \rightarrow p\mu^+\mu^-)$ and the real parts of a and b .

in the third column of the table, is still compatible with the PDG value at the two-sigma level [67] if both of their errors are taken into account. We expect that the situation will become clearer [67] when an improved result from LHCb becomes available in the near future. [67]

Measurements of the branching fraction of $\Sigma^+ \rightarrow pe^+e^-$ may offer an additional way to [69] resolve the fourfold ambiguity. In this mode, the dominance of the LD contributions is more [69] pronounced, owing to the fact that the a and b terms in the amplitude are much enhanced at low [69] values of the dielectron invariant mass, $M_{ee} = \sqrt{q^2} \geq 2m_e$. As a consequence, the predictions [69] for $\mathcal{B}_{ee} = \mathcal{B}(\Sigma^+ \rightarrow pe^+e^-)$ corresponding to the various solutions are similar to one another, as [69] can be seen in the sixth column of Table I. Nevertheless, the difference between solutions can be [69] magnified by raising the minimum of M_{ee} . This might be achieved by applying, for instance, the [69] cut $M_{ee} \geq 100$ MeV, leading to the numbers in the last column of Table I. Thus, the selection [69] of an appropriate lower bound on M_{ee} could make the predictions of the different solutions more [69] distinguishable. This point is further illustrated by Fig. 2. Although the implementation of the [69] $M_{ee\min}$ cut has a price, which is a decreased rate, the latter may still be within the sensitivity [69] reach of BESIII [2] and LHCb [3–5], depending on the choice of $M_{ee\min}$. [69]

It is worth remarking here that the \mathcal{B}_{ee} range in the sixth column of Table I is roughly 20% less [70] than the corresponding predictions made in Refs. [8, 38]. This is largely because of our adoption [70] of the BESIII finding of \mathcal{B}_γ quoted in Eq. (10), which is also $\sim 20\%$ lower than the present PDG [70] average [17]. The empirical information on $\Sigma^+ \rightarrow pe^+e^-$ is still scarce. From the only existing [70] data, reported in Ref. [22], one can infer $\mathcal{B}(\Sigma^+ \rightarrow pe^+e^-) = (7.7 \pm 4.6) \times 10^{-6}$ [8],⁴ which is far [70] from precise and accommodates well all the \mathcal{B}_{ee} predictions in the sixth column of Table I. Thus, [71]

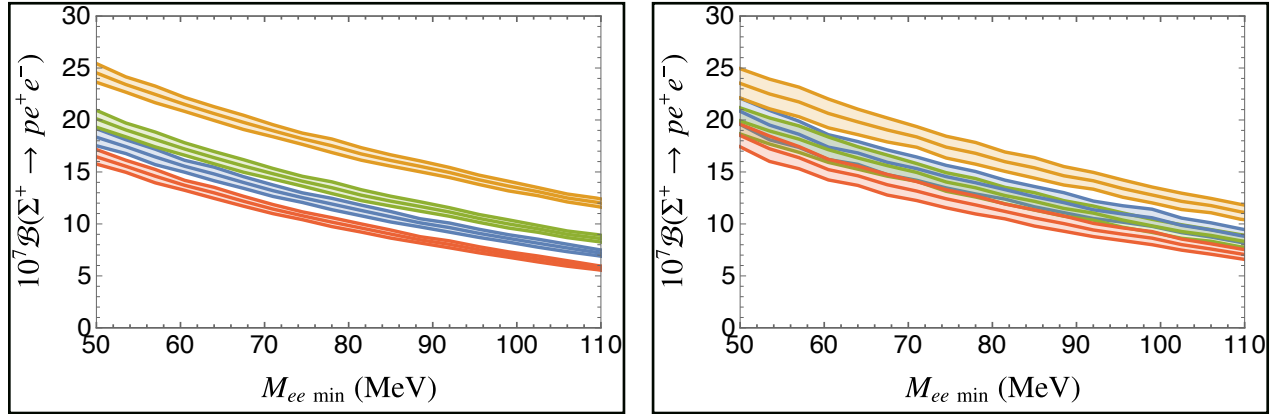


FIG. 2. Dependence of the SM branching fraction of $\Sigma^+ \rightarrow pe^+e^-$ on a minimum cut in the dielectron [68] invariant mass for the four solutions obtained with relativistic baryon χ PT (left plot) and with its [68] heavy-baryon formulation (right plot). In all of the figures in this section, the blue, yellow, green, and [68] red colors correspond to solutions 1, 2, 3, and 4, respectively. The band of each curve in this and the [68] next three figures reflects the ranges of $\text{Re}(a, b)$ and $\text{Im}(a(0), b(0))$ for the corresponding solution. [68]

⁴ The PDG limit $\mathcal{B}(\Sigma^+ \rightarrow pe^+e^-) < 7 \times 10^{-6}$ [17] is for neutral currents in this mode and not for its full [70] branching fraction [22]. [70]

it goes without saying that the upcoming measurements of $\Sigma^+ \rightarrow p e^+ e^-$ by BESIII and LHCb⁷¹ can be anticipated to provide highly desirable information pertinent to our study.⁷¹

Returning to the $\ell = \mu$ case, one can write the double differential distribution [38, 39]⁷²

$$\frac{d^2\Gamma(\Sigma^+ \rightarrow p\mu^+\mu^-)}{dq^2 d(\cos\theta_\mu)} = \left[\frac{3}{8} \left(1 + \cos^2\theta_\mu \right) \left(1 - f_L \right) + \mathcal{A}_{FB} \cos\theta_\mu + \frac{3}{4} f_L \sin^2\theta_\mu \right] \frac{d\Gamma(\Sigma^+ \rightarrow p\mu^+\mu^-)}{dq^2}$$

$$= \mathcal{F}_0 + \mathcal{F}_1 \cos\theta_\mu + \mathcal{F}_2 \cos^2\theta_\mu,$$
(16) 64 70

where θ_μ stands for the angle between the directions of the μ^- and p in the rest frame of the $\mu^+\mu^-$ system, f_L is the fraction of longitudinally polarized dimuons, \mathcal{A}_{FB} designates the muon forward-backward asymmetry, and f_L , \mathcal{A}_{FB} , and $\mathcal{F}_{0,1,2}$ are all independent of θ_μ . The expressions for $\mathcal{F}_{0,1,2}$ in the general parameterization of Eq. (14) can be found in the appendix of Ref. [38].⁷⁴

Thus, explicitly we have [38]⁷⁵

$$\mathcal{A}_{FB} = \frac{\beta^2 \bar{\lambda}}{64\pi^3 \Gamma' m_\Sigma^3} \text{Re} \left\{ \left[M_+ \tilde{A}^* \tilde{F} - M_- \tilde{B}^* \tilde{E} - (\tilde{A}^* \tilde{G} + \tilde{B}^* \tilde{H}) m_\mu + \tilde{C}^* \tilde{F} + D^* \tilde{E} \right] q^2 \right.$$

$$\left. - (M_+ \tilde{C}^* \tilde{G} - M_- \tilde{D}^* \tilde{H}) m_\mu \right\},$$
(17) 64 70

where⁶¹

$$\Gamma' \equiv \frac{d\Gamma(\Sigma^+ \rightarrow p\mu^+\mu^-)}{dq^2} = 2\mathcal{F}_0 + \frac{2}{3}\mathcal{F}_2, \quad \beta = \sqrt{1 - \frac{4m_\mu^2}{q^2}} \quad 52 \quad 190 \quad 107$$

$$\bar{\lambda} = (M_+^2 - q^2)(M_-^2 - q^2), \quad M_\pm = m_\Sigma \pm m_\mu. \quad (18) 78$$

Since \tilde{A} , \tilde{B} , \tilde{C} , and \tilde{D} are dominated by the LD contributions, while \tilde{E} , \tilde{F} , \tilde{G} , and \tilde{H} are not,⁷⁹ \mathcal{A}_{FB} is potentially sensitive to NP which can enhance one or more of the latter set of quantities⁷⁹ significantly compared to their SM expectations. Also of interest is the integrated forward-backward asymmetry⁷⁹

$$\tilde{A}_{FB} = \frac{1}{\Gamma(\Sigma^+ \rightarrow p\mu^+\mu^-)} \int \Gamma' \mathcal{A}_{FB} dq^2,$$
(19) 64 70

where both the numerator and denominator of \tilde{A}_{FB} are to be evaluated for the same solution.⁸¹ The SM prediction for \tilde{A}_{FB} can be viewed in the fifth column of Table I, and its differential distribution,⁸¹

$$\frac{d\tilde{A}_{FB}}{dM_{\mu\mu}} = \frac{2\Gamma' \mathcal{A}_{FB} M_{\mu\mu}}{\Gamma(\Sigma^+ \rightarrow p\mu^+\mu^-)},$$
(20) 80

versus the dimuon invariant mass $M_{\mu\mu} = \sqrt{q^2}$ is depicted in Fig. 3. Evidently, there is a sign flip for two of the solutions (distributions 1 and 2 in both the relativistic and heavy-baryon cases⁸³ become negative).⁸³

Another important quantity is the dimuon spectrum given by⁸⁶

$$\frac{1}{\hat{\Gamma}} \frac{d\hat{\Gamma}}{dM_{\mu\mu}} = \frac{2\Gamma' M_{\mu\mu}}{102 \quad 73 \quad 76} \hat{\Gamma} \equiv \Gamma(\Sigma^+ \rightarrow p\mu^+\mu^-),$$
(21) 64 70

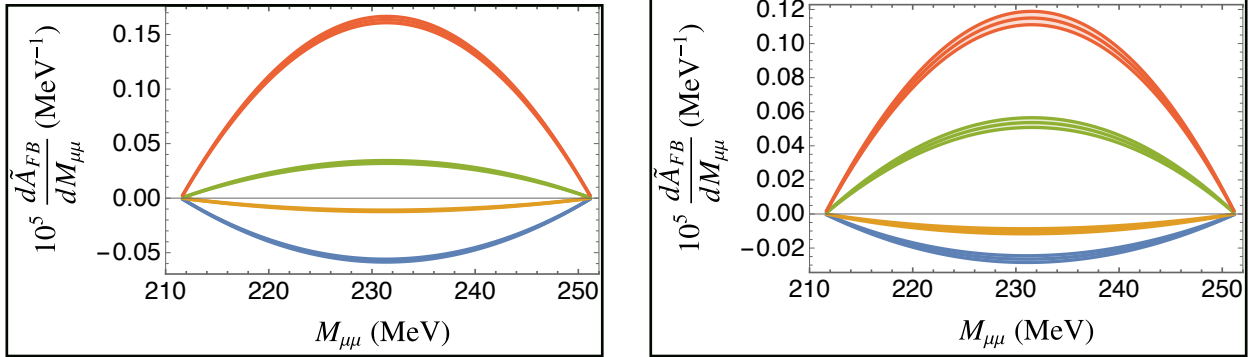


FIG. 3. The differential \tilde{A}_{FB} distribution in $\Sigma^+ \rightarrow p\mu^+\mu^-$ versus the dimuon invariant mass, $M_{\mu\mu}$, for [84] the four relativistic (left) and heavy-baryon (right) solutions in the SM. [84]

hence also normalized by the rate. The dependence of $(d\hat{\Gamma}/dM_{\mu\mu})/\hat{\Gamma}$ on $M_{\mu\mu}$ for each of the [88] solutions is illustrated in Fig. 4. It can be seen that the spectrum for solution 4, in both the [88] relativistic and heavy-baryon cases, peaks at lower $M_{\mu\mu}$ than the other three. [88]

From the two lines in Eq. (16), it is straightforward to realize that the fraction f_L of longitudinally [89] polarized dimuons is related to $\mathcal{F}_{0,2}$ by [89]

$$f_L = \frac{2}{3\hat{\Gamma}} (\mathcal{F}_0 - \mathcal{F}_2) \quad [22] 107 \quad 101$$

where $\Gamma' = 2\mathcal{F}_0 + 2\mathcal{F}_2/3$ with the \mathcal{F}_0 term being numerically dominant, as detailed in Ref. [38]. [91]
We can then define the integrated form [91]

$$\hat{f}_L = \frac{1}{\hat{\Gamma}} \int \Gamma' f_L q^2 = \frac{4}{3\hat{\Gamma}} \int (\mathcal{F}_0 - \mathcal{F}_2) M_{\mu\mu} dM_{\mu\mu}. \quad [23] 107 \quad 101$$

In Fig. 5 we display $d\hat{f}_L/dM_{\mu\mu}$ versus $M_{\mu\mu}$. This distribution mostly mimics the dimuon spectrum [93] in Fig. 4, which is expected due to the numerical smallness of \mathcal{F}_2 relative to \mathcal{F}_0 within the SM. [93]
It is interesting to mention that experimentally it may be possible to extract f_L from Eq. (16), [93]
as was done for $\Lambda_b \rightarrow \Lambda\mu^+\mu^-$ by LHCb [39]. [90]

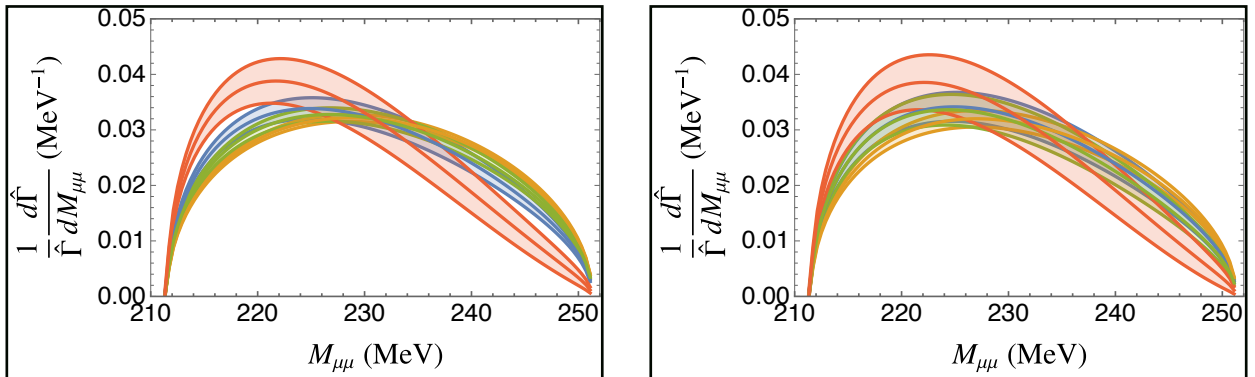


FIG. 4. The dimuon spectrum in $\Sigma^+ \rightarrow p\mu^+\mu^-$ versus the dimuon invariant mass for the four relativistic [85] (left) and heavy-baryon (right) solutions in the SM. [85]

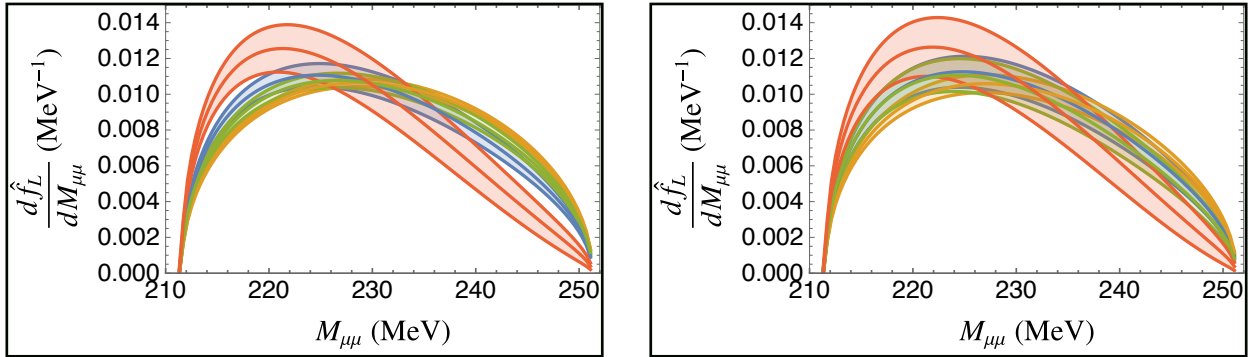


FIG. 5. The \hat{f}_L distributions in $\Sigma^+ \rightarrow p\mu^+\mu^-$ in the SM normalized to their corresponding rate for the four relativistic (left) and heavy-baryon (right) solutions.⁹⁴

V. NEW PHYSICS CONTRIBUTIONS^{91 100 101}

To take into account the effects of new physics beyond the SM, we work with the effective Hamiltonian⁹⁶

$$\mathcal{H}_{\text{eff}} = - \sum_i \mathcal{C}_i \mathcal{O}_i + \text{H.c.}, \quad (24)$$
93

where the operators \mathcal{O}_i are defined as⁹⁸

$\mathcal{O}_7 = \frac{\lambda_t G_F}{\sqrt{2}} \frac{e m_s}{4\pi^2} \bar{s}_R \sigma^{\kappa\nu} d_L F_{\kappa\nu},$ $\mathcal{O}_9^\ell = \frac{\lambda_t G_F}{\sqrt{2}} \frac{e^2}{4\pi^2} \bar{s}_L \gamma^\nu d_L \bar{\ell} \gamma_\nu \ell,$ $\mathcal{O}_{10}^\ell = \frac{\lambda_t G_F}{\sqrt{2}} \frac{e^2}{4\pi^2} \bar{s}_L \gamma^\nu d_L \bar{\ell} \gamma_\nu \gamma_5 \ell,$ $\mathcal{O}_S = \frac{\lambda_t G_F}{\sqrt{2}} \frac{e^2 m_s}{4\pi^2} \bar{s}_L d_R \bar{\ell} \ell,$ $\mathcal{O}_P = \frac{\lambda_t G_F}{\sqrt{2}} \frac{e^2 m_s}{4\pi^2} \bar{s}_L d_R \bar{\ell} \gamma_5 \ell,$	$\mathcal{O}_{7'} = \frac{\lambda_t G_F}{\sqrt{2}} \frac{e m_s}{4\pi^2} \bar{s}_L \sigma^{\kappa\nu} d_R F_{\kappa\nu},$ $\mathcal{O}_{9'}^\ell = \frac{\lambda_t G_F}{\sqrt{2}} \frac{e^2}{4\pi^2} \bar{s}_R \gamma^\nu d_R \bar{\ell} \gamma_\nu \ell,$ $\mathcal{O}_{10'}^\ell = \frac{\lambda_t G_F}{\sqrt{2}} \frac{e^2}{4\pi^2} \bar{s}_R \gamma^\nu d_R \bar{\ell} \gamma_\nu \gamma_5 \ell,$ $\mathcal{O}_{S'} = \frac{\lambda_t G_F}{\sqrt{2}} \frac{e^2 m_s}{4\pi^2} \bar{s}_R d_L \bar{\ell} \ell,$ $\mathcal{O}_{P'} = \frac{\lambda_t G_F}{\sqrt{2}} \frac{e^2 m_s}{4\pi^2} \bar{s}_R d_L \bar{\ell} \gamma_5 \ell,$
--	---

(25)
99

with $f_{L,R} = P_{L,R} f$ for fermion f and $\lambda_q = V_{qd} V_{qs}^*$. For the Wilson coefficients \mathcal{C}_i in Eq. (24), we explicitly separate any SM contribution to them by writing $\mathcal{C}_i = C_i^{\text{SM}} + C_i$, where " C_i " designates the part induced by NP. Since we consider only NP that preserves CP symmetry, we suppose that the products $\lambda_j C_i$, which occur in \mathcal{H}_{eff} , are real numbers. As seen below, the C_i enter the kaon observables of interest as either of $C_{j\pm} \equiv (C_j \pm C_{j'})$, $j = 7, 9, 10, S, P$, and so we will adopt those combinations.¹⁰⁰

From the H.c. part of \mathcal{H}_{eff} in Eq. (24), the NP contributions to $\Sigma^+ \rightarrow p\ell^+\ell^-$ are [101 107 63]

$$\begin{aligned} \tilde{A} &= \frac{\lambda_t G_F}{\sqrt{2}} \frac{e^2 m_s}{4\pi^2 q^2} c_\sigma C_{7+}, & \tilde{B} &= \frac{\lambda_t G_F}{\sqrt{2}} \frac{e^2 m_s}{4\pi^2 q^2} c_\sigma C_{7-}, \\ \tilde{C} &= \frac{-\lambda_t G_F}{\sqrt{2}} \frac{e^2}{8\pi^2} C_{9+}, & \tilde{D} &= \frac{\lambda_t G_F}{\sqrt{2}} \frac{e^2}{8\pi^2} (F - D) C_{9-}, \\ \tilde{E} &= \frac{\lambda_t G_F}{\sqrt{2}} \frac{e^2}{8\pi^2} C_{10+}, & \tilde{F} &= \frac{\lambda_t G_F}{\sqrt{2}} \frac{e^2}{8\pi^2} (D - F) C_{10-}, \\ \tilde{G} &= \frac{\lambda_t G_F}{\sqrt{2}} \frac{e^2 m_s}{8\pi^2} \left(\frac{m_\Sigma - m_p}{m_s - m_d} \right) C_{S+}, & \tilde{J} &= \frac{\lambda_t G_F}{\sqrt{2}} \frac{e^2 m_s}{8\pi^2} \left(\frac{m_\Sigma - m_p}{m_d - m_s} \right) C_{P+}, \end{aligned} \quad (26)$$

[102]

and [103]

$$\begin{aligned} \tilde{H} &= \frac{\lambda_t G_F}{\sqrt{2}} \frac{e^2 m_s}{8\pi^2} \left(\frac{m_\Sigma + m_p}{m_{K^0}^2 - q^2} \right) \frac{m_{K^0}^2}{m_d + m_s} (D - F) C_{S-}, \\ \tilde{K} &= \frac{\lambda_t G_F}{\sqrt{2}} \frac{e^2}{8\pi^2} \left(\frac{m_\Sigma + m_p}{q^2 - m_{K^0}^2} \right) (D - F) \left(2C_{10-} m_\ell + \frac{C_{P-} m_{K^0}^2 m_s}{m_d + m_s} \right), \end{aligned} \quad (27)$$

[104]

where the relation $\lambda_t^* C_i^* = \lambda_t C_i$ has been applied, which is valid for $\text{Im}(\lambda_t C_i) = 0$. In numerical work we set $e^2 = 4\pi\alpha_e(0)$ for the a, b, c , and d terms in Eq. (15), which arise from photon-exchange LD effects, and $e^2 = 4\pi\alpha_e(m_Z)$ in the rest of Eq. (15) and in Eqs. (26)-(27). [105]

The complete numerical expression for $\mathcal{B}(\Sigma^+ \rightarrow p\mu^+\mu^-)$ can be written as [106]

$$\mathcal{B}(\Sigma^+ \rightarrow p\mu^+\mu^-)_i = \left[\text{SM}_i + \sum_j n_{ij} (\lambda_t C_j) \right] \times 10^{-8}, \quad (28)$$

[108]

where SM_i refers to each of the four solutions derived with relativistic baryon χ PT and with its heavy-baryon formulation. The terms linear in the Wilson coefficients (WCs) representing NP arise from interference with the SM and are therefore different for each case. These terms are largest when the WCs interfere with the SM long-distance component. The part quadratic in the WCs, $C_j C_k$, originate purely from NP and are thus the same for all four solutions. We display our numerical results for n_{ij} and q_{jk} in Tables II and III,⁵ respectively. These numbers indicate that, with λ_t multiplying each WC in Eq. (28), the dimensionless ones, such as C_{7-} and C_{9-} , must be at least a few times 10^2 in size to modify the SM rates at the percent level or higher.⁶ [108]

We now turn our attention to the integrated forward-backward asymmetry as defined in Eq. (19) in the presence of NP. The decay rate that normalizes this asymmetry also varies when there is NP, as per Eq. (28), but we present results that include the NP terms only in the

⁵ Ref. [40] gives a result that includes only the C_{9+}^2 and C_{9-}^2 . Our numbers disagree with theirs by factors of two. Converting their result to our notation, they find coefficients 1.94 for C_{9+}^2 and 0.94 for C_{9-}^2 instead of our 0.972 and 2.06, respectively, from Table III. [108]

⁶ Equivalently, only NP arising from ultraviolet models without a mixing angle suppression similar to λ_t can measurably affect this rate. [108]

Solution	SM _i	C ₇₊	C ₇₋	C ₉₊	C ₉₋
Rel 1	2.7	-0.070	0.34	0.046	0.37
Rel 2	7.8	-0.028	0.71	0.026	0.77
Rel 3	4.2	0.025	-0.50	-0.0008	-0.55
Rel 4	1.2	0.067	-0.14	-0.021	-0.15
HB 1	3.6	-0.057	0.40	0.040	0.44
HB 2	6.2	-0.035	0.59	0.029	0.65
HB 3	3.2	0.032	-0.39	-0.0043	-0.42
HB 4	1.8	0.054	-0.20	-0.015	-0.21

TABLE II. Numerical coefficients SM_i and n_{ij} appearing in Eq. (28). [109, 110]

C ₇₊ ²	C ₇₋ ²	C ₉₊ ²	C ₉₋ ²	C ₁₀₊ ²	C ₁₀₋ ²	C _{S+} ²	C _{S-} ²	C _{P+} ²	C _{P-} ²
0.194	1.73	0.972	2.06	5.6	0.41	0.06 GeV ²	0.0013 GeV ²	0.353 GeV ²	0.01 GeV ²

C ₇₊ C ₉₊	C ₇₋ C ₉₋	C ₁₀₊ C _{P+}	C ₁₀₋ C _{P-}
-0.193	3.75	-2.78 GeV	0.082 GeV

TABLE III. Numerical coefficients q_{jk} appearing in Eq. (28). [107, 97, 99]

numerator of the asymmetry. The rationale for this choice is that this observable will only be measured after the decay rate is known. With this in mind, we write for the terms that arise from interference with the LD SM contribution as

$$\tilde{A}_{\text{FB}} = \frac{1}{\Gamma(\Sigma^+ \rightarrow p\mu^+\mu^-)} \int \Gamma' \mathcal{A}_{\text{FB}} dq^2 \supset [a_{10+} (\lambda_t C_{10+}) + a_{10-} (\lambda_t C_{10-}) + a_{S+} \text{GeV} (\lambda_t C_{S+}) + a_{S-} \text{GeV} (\lambda_t C_{S-})] \times 10^{-2}, \quad (29)$$

where the coefficients a_i for the four relativistic solutions and their heavy-baryon counterparts are tabulated in Table IV.⁷ With NP coefficients of order 10², their impact is to cause \tilde{A}_{FB} to exceed its SM expectations by a factor of ten already.

Solution	a ₁₀₊	a ₁₀₋	a _{S+}	a _{S-}
Rel 1	-0.22 ± 0.01	-1.18 ± 0.02	0.082 ± 0.001	-0.092 ± 0.006
Rel 2	-0.158 ± 0.003	-0.16 ± 0.01	0.020 ± 0.001	-0.065 ± 0.001
Rel 3	0.214 ± 0.005	0.29 ± 0.03	0.015 ± 0.001	0.083 ± 0.002
Rel 4	0.20 ± 0.03	2.54 ± 0.05	-0.003 ± 0.002	0.07 ± 0.01
HB 1	-0.19 ± 0.02	-0.70 ± 0.04	0.054 ± 0.001	-0.081 ± 0.007
HB 2	-0.16 ± 0.01	-0.26 ± 0.03	0.026 ± 0.001	-0.067 ± 0.003
HB 3	0.21 ± 0.01	0.47 ± 0.06	0.016 ± 0.002	0.078 ± 0.006
HB 4	0.20 ± 0.03	1.36 ± 0.08	0.010 ± 0.003	0.07 ± 0.01

TABLE IV. Coefficients a_i in Eq. (19) for the integrated forward-backward asymmetry. [115]

⁷ These numbers appear in Ref. [40] for one relativistic solution, and when converted to our conventions they disagree with ours. That reference comments that this is due to the use of different form factors. [116]

The additional terms in \tilde{A}_{FB} , besides those in the second line of Eq. (29), are expressible as 120

$$\Gamma(\Sigma^+ \rightarrow p\mu^+\mu^-) \tilde{A}_{\text{FB}} \supset \sum_{ij} [\tilde{q}_{ij} (\lambda_t C_i)(\lambda_t C_j) \times 10^{-25}], \quad (30) \quad 130$$

and therefore the parameters \tilde{q}_{ij} are independent of the SM LD effects. Our numerical results 122 for \tilde{q}_{ij} can be viewed in Table V. 122

$C_{7+}C_{10-}$	$C_{7+}C_{S+}$	$C_{7-}C_{10+}$	$C_{7-}C_{S-}$	$C_{9+}C_{10-}$	$C_{9+}C_{S+}$	$C_{9-}C_{10+}$	$C_{9-}C_{S-}$
1.5	-0.052 GeV	-0.49	-0.20 GeV	-0.51	1.5 GeV	-0.51	-0.24 GeV

TABLE V. Numerical coefficients \tilde{q}_{ij} appearing in Eq. (30). 107 104 115

VI. KAON OBSERVABLES 146 133 137

A. SM Wilson coefficients 127

The kaon modes affected by the quark-level transition $s \rightarrow d\mu^+\mu^-$ are also dominated by long-distance contributions within the SM. This makes it very difficult to extract precise information 128 on the SM short-distance parameters, or, indeed, new physics. Nevertheless, the corresponding 128 kaon data can serve as useful constraints on NP which is large enough to measurably affect the 128 $\Sigma^+ \rightarrow p\mu^+\mu^-$ rate. The SM SD contributions enter these modes via the Wilson coefficients, at 128 the scale $\mu = 1 \text{ GeV}$. 128

$$C_7^{\text{SM}} = \frac{-\lambda_u}{2\lambda_t} C_{7\gamma}, \quad C_9^{\text{SM}} = \frac{2\pi}{\alpha_e} \left(y_{7V} - \frac{\lambda_u}{\lambda_t} z_{7V} \right), \quad C_{10}^{\text{SM}} = \frac{2\pi}{\alpha_e} y_{7A}. \quad (31) \quad 129$$

Numerically we employ $z_{7V} = -0.046\alpha_e$, $y_{7V} = 0.73\alpha_e$, and $y_{7A} = -0.68\alpha_e$, as before.⁸ 70 199 119

B. Relevant kaon modes 131

We begin with the modes $K_{L,S} \rightarrow \mu^+\mu^-$. For our numerical study, we employ the expressions 132 for all contributions to these two rates that exist in the public SuperIso code [42, 43]. In both 132 cases, the LD contribution is dominated by a two-photon intermediate state. Its extraction relies 132 on the measured $K_{L,S} \rightarrow \gamma\gamma$ rates supplemented with hadronic models. The LD contributions 132 to $K_{L,S} \rightarrow \mu^+\mu^-$ are therefore potentially contaminated by NP entering through $C_{7,7'}$. This has 132 been considered in the literature, and we will later list the corresponding constraints obtained 132 in Ref. [44], on Table VII. There are several proposals to improve these measurements [7]. 132

⁸ The error in these coefficients is sometimes quantified as $y_{7V} = (0.73 \pm 0.04)\alpha_e$ and $y_{7A} = (-0.68 \pm 0.03)\alpha_e$, with the uncertainty range arising from taking $\bar{m}_t(m_t) = (167 \pm 5) \text{ GeV}$ and $0.8 \leq \mu/\text{GeV} \leq 1.2$ [41]. 130

1. $K_L \rightarrow \mu^+ \mu^-$ [115 121 129]

This mode receives a SD contribution proportional to $\text{Re } C_{10}^{\text{SM}}$, but the rate is dominated by the aforesaid LD contribution from a two-photon intermediate state. The absorptive part of this LD contribution is determined by the measured rate of $K_L \rightarrow \gamma\gamma$, and the difference between this rate and the absorptive contribution can be attributed to a combination of a model-dependent LD dispersive contribution, a SM SD contribution, and NP. The branching fraction in relation to all of them can be parameterized as [18, 45] [134]

$$\mathcal{B}(K_L^0 \rightarrow \mu^+ \mu^-) = \tau_{K_L} \frac{f_K^2 m_{K^0}^3 \beta_{\mu, K}}{16\pi} (|N_L^{\text{LD}} + A_L^{\text{SM}} + A_L^{\text{NP}}|^2 + \beta_{\mu, K}^2 |B_L|^2),$$

$$N_L^{\text{LD}} = \pm [0.54(77) - 3.95i] \times 10^{-11} \text{ GeV}^{-2},$$

$$A_L^{\text{SM}} = \frac{G_F \alpha_e}{\sqrt{2}\pi} \frac{2m_\mu}{m_{K^0}} \left(\frac{Y_c}{s_W^2} \text{Re } \lambda_c + \frac{Y(x_t)}{s_W^2} \text{Re } \lambda_t \right) [17 21 26],$$

$$A_L^{\text{NP}} = \frac{-G_F \alpha_e}{\sqrt{2}\pi} \text{Re} \left[\frac{2m_\mu}{m_{K^0}} (\lambda_t C_{10-}) + \frac{m_{K^0} m_s}{m_s + m_d} (\lambda_t C_{P-}) \right] [47 210 211] (32) [37 64],$$

$$B_L = \frac{G_F \alpha_e}{\sqrt{2}\pi} \frac{m_{K^0} m_s}{(m_s + m_d)} \text{Im} (\lambda_t C_{S-}).$$
135

Recall that we are assuming no CP violation in the NP for our numerical study, implying that we set $B_L = 0$. We have explicitly separated the SM SD contribution, A_L^{SM} [46], so that C_{10} refers to NP only. [136]

2. $K_S \rightarrow \mu^+ \mu^-$ [137 133 122]

This mode also has SD and LD components entering the branching fraction as [18, 45] [138]

$$\mathcal{B}(K_S^0 \rightarrow \mu^+ \mu^-) = \tau_{K_S} \frac{f_K^2 m_{K^0}^3 \beta_{\mu, K}}{16\pi} (\beta_{\mu, K}^2 |N_S^{\text{LD}} - A_S^{\text{NP}}|^2 + |B_S^{\text{SM}} + B_S^{\text{NP}}|^2),$$

$$N_S^{\text{LD}} = (-2.65 + 1.14i) \times 10^{-11} \text{ GeV}^{-2},$$

$$A_S^{\text{NP}} = \frac{G_F \alpha_e}{\sqrt{2}\pi} \frac{m_{K^0} m_s}{(m_s + m_d)} \text{Re} (\lambda_t C_{S-}),$$

$$B_S^{\text{SM}} = \frac{G_F \alpha_e}{\sqrt{2}\pi} \frac{2m_\mu}{m_{K^0}} \text{Im} \left(\frac{-Y_c}{s_W^2} \lambda_c - \frac{Y(x_t)}{s_W^2} \lambda_t \right) [65 91 122 117],$$

$$B_S^{\text{NP}} = \frac{G_F \alpha_e}{\sqrt{2}\pi} \left[\frac{2m_\mu}{m_{K^0}} \text{Im} (\lambda_t C_{10-}) + \frac{m_{K^0} m_s}{m_s + m_d} \text{Im} (\lambda_t C_{P-}) \right] [103 105] (33) [190 107].$$
139

Again, we have explicitly written the SM SD contribution through C_{10} as B_S^{SM} . In the scenario with no CP violation in the NP, $B_S^{\text{NP}} = 0$. [140]

3. $K_{L,S} \rightarrow \pi^0 \ell^+ \ell^-$ [141]

Within the SM these modes are predominantly CP -violating and receive multiple contributions. There are direct and through-mixing CP -violating contributions as well as interference

between them, $C_{\text{dir}}^{\ell\ell}$, $C_{\text{mix}}^{\ell\ell}$ and $C_{\text{int}}^{\ell\ell}$ respectively. Theoretical considerations suggest that the sign of the interference term is plus [47]. There is also a LD CP -conserving contribution dominated by a two-photon intermediate state,⁹ $C_{\gamma\gamma}^{\ell\ell}$. Potentially there are NP contributions as well, which we include following Ref. [48]. Some enter $C_{\text{dir}}^{\ell\ell}$ and others we dub $C_{\text{NP}}^{\ell\ell}$. A practical complication when using these modes to constrain NP is that two contributions are extracted from experiment. The CP -conserving contribution is partially extracted from $K_L \rightarrow \pi^0 \gamma\gamma$ and as such is potentially contaminated by NP through $C_{7,7'}$. We partially address this issue by using the constraints on C_7 and $C_{7'}$ as obtained from the $K \rightarrow \pi\pi\gamma$ and $K \rightarrow \gamma\gamma$ modes [44], respectively. The CP -violating contribution through mixing relies on the measurement of $K_S \rightarrow \pi^0 \ell^+ \ell^-$, and NP affecting those modes could contaminate the extracted value of a_S . However, an a_S representing LD contributions is the same for both the electron and muon modes, so that the difference between the two extractions can be attributed to NP that breaks lepton flavor universality (LFU). 142

We follow Refs. [41, 47–49] to write 143

$$\mathcal{B}(K_L \rightarrow \pi^0 \ell\bar{\ell}) = (C_{\text{NP}}^{\ell\ell} + C_{\text{dir}}^{\ell\ell} \pm C_{\text{int}}^{\ell\ell} |a_S| + C_{\text{mix}}^{\ell\ell} |a_S|^2 + C_{\gamma\gamma}^{\ell\ell}) \times 10^{-12}. \quad (34) \quad 144$$

As the expressions below imply, NP contributions may enter the rate through the term $C_{\text{NP}}^{\ell\ell}$ via the coefficients C_{P+} and C_{S+} and also through the term $C_{\text{dir}}^{\ell\ell}$ via the coefficients C_{9+} and C_{10+} . 145

To exhibit the dependence of the first three terms in Eq. (34) on the possible NP, we follow Refs. [48, 49] and write¹⁰ 146

$$\begin{aligned} C_{\text{NP}}^{\mu\mu} &= 10^8 \text{Im}(\lambda_t C_{P+} \text{GeV}) \{ 0.09 \text{Im} \lambda_t + [0.0039 \text{Im}(\lambda_t C_{P+} \text{GeV}) - 0.02 \text{Im}(\lambda_t C_{10+})] \}, \\ &\quad + 10^4 \text{Re}(\lambda_t C_{S+} \text{GeV}) [-0.027(7) + 0.0019 \times 10^4 \text{Re}(\lambda_t C_{S+} \text{GeV})], \\ C_{\text{dir}}^{\mu\mu} &= 10^8 \{ 0.033 [\text{Im}(\lambda_t C_{10+}) - 4.27(19) \text{Im} \lambda_t]^2 + 0.014 [\text{Im}(\lambda_t C_{9+}) + 4.59(25) \text{Im} \lambda_t]^2 \}, \\ C_{\text{int}}^{\mu\mu} &= 10^4 [1.37(8) \text{Im} \lambda_t + 0.3 \text{Im}(\lambda_t C_{9+})], \\ C_{\text{NP}}^{ee} &= 10^8 \text{Im}(\lambda_t C_{P+} \text{GeV}) \{ 0.0013 \text{Im} \lambda_t + [0.0076 \text{Im}(\lambda_t C_{P+} \text{GeV}) - 0.0003 \text{Im}(\lambda_t C_{10+})] \}, \\ &\quad + 10^4 \text{Re}(\lambda_t C_{S+} \text{GeV}) [-0.021(4) + 0.0077 \times 10^4 \text{Re}(\lambda_t C_{S+} \text{GeV})], \\ C_{\text{dir}}^{ee} &= 0.06 \times 10^8 \{ [\text{Im}(\lambda_t C_{10+}) - 4.27(19) \text{Im} \lambda_t]^2 + [\text{Im}(\lambda_t C_{9+}) + 4.59(25) \text{Im} \lambda_t]^2 \}, \\ C_{\text{int}}^{ee} &= 10^4 [5.84(35) \text{Im} \lambda_t + 1.28 \text{Im}(\lambda_t C_{9+})], \end{aligned} \quad (35) \quad 148$$

where the terms linear in $\text{Re} C_{S+}$ arise from interference with the two-photon contribution. In Eq. (35) the explicit factors of 10^4 and 10^8 appear from the practice of writing this result in terms of $10^4 \lambda_t$. In addition, the last two terms in Eq. (34) are given by 148

$$C_{\text{mix}}^{\mu\mu} = 3.36 \pm 0.20, \quad C_{\gamma\gamma}^{\mu\mu} = 5.2 \pm 1.6, \quad C_{\text{mix}}^{ee} = 14.5 \pm 0.5, \quad C_{\gamma\gamma}^{ee} \approx 0. \quad (36) \quad 149$$

⁹ For our numerical studies we will use the expressions for these modes as coded for **SuperIso** and provided to us by F. Mahmoudi. 142

¹⁰ It is to be understood that the WCs contributing to the various dielectron and dimuon observables need to have superscripts $\ell\ell = ee$ and $\mu\mu$, respectively, if LFU is absent and the two types of WCs occur together and are both nonzero, as in a few instances discussed below. In our numerical analysis in Sec. VII we assume that only the $\ell = \mu$ WCs contain NP. 146

In the scenario we are pursuing here, where the NP is CP conserving, these results indicate that [150](#)
 C_{S+} is the only WC that can be constrained by these modes. [150](#)

However, it is also possible for NP to contaminate the extraction of the parameter a_S , and [151](#)
in that way a constrain on C_{9+} arises. The parameter a_S can be inferred from measurements [151](#)
of $K_S \rightarrow \pi^0 \ell^+ \ell^-$. Those modes, in turn, are LD dominated and parameterized in χ PT with [151](#)
the constants a_S and b_S which are then extracted from experiment [\[50, 51\]](#). Early extractions [151](#)
assuming LFU suggested the value $|a_S| = 1.20 \pm 0.20$ [\[41\]](#), whereas more recent studies suggest [151](#)
a larger error, $|a_S| = 1.3 \pm 3.2$ [\[52\]](#). [151](#)

A contamination from NP can only be extracted from these if it violates LFU. The separate [152](#)
measurements of a_S in the muon and electron modes start from the χ PT parameterization of the [152](#)
LD SM branching fractions given by [\[53\]](#) [152](#)

$$\begin{aligned} \mathcal{B}(K_S \rightarrow \pi^0 e^+ e^-) &= (0.01 - 0.55a_S - 0.17b_S + 43.76a_S^2 + 11.83a_S b_S + 1.28b_S^2) \times 10^{-10}, \\ \mathcal{B}(K_S \rightarrow \pi^0 \mu^+ \mu^-) &= (0.07 - 3.96a_S - 1.34b_S + 86.90a_S^2 + 50.21a_S b_S + 7.66b_S^2) \times 10^{-11}. \end{aligned} \quad (37) \quad \text{153}$$

Existing measurements do not have enough information to determine both a_S and b_S , and so [154](#)
predictions rely on a vector-meson-dominance model leading to $b_S/a_S = m_K^2/m_\rho^2$ [\[51\]](#). Using [154](#)
this form, the experimental collaborations have extracted a value for a_S from each of the two [154](#)
modes [\[54, 55\]](#), [154](#)

$$\begin{aligned} a_S \text{ from } K_S \rightarrow \pi^0 e^+ e^- &\quad 1.06^{+0.26}_{-0.21} \pm 0.07, \\ a_S \text{ from } K_S \rightarrow \pi^0 \mu^+ \mu^- &\quad 1.54^{+0.40}_{-0.32} \pm 0.06. \end{aligned} \quad \text{155}$$

(38) [134](#) [135](#)

With these two numbers, one can constrain the combination $C_{9+}^{\mu\mu} \text{156} C_{9+}^{ee}$ via

$$a_S^{\mu\mu} - a_S^{ee} = -\sqrt{2} \operatorname{Re}[V_{td} V_{ts}^* (C_{9+}^{\mu\mu} - C_{9+}^{ee})] = -\sqrt{2} |\lambda_t| (C_{9+}^{\mu\mu} - C_{9+}^{ee}) = 0.5 \pm 0.5. \quad (39) \quad \text{157}$$

A forward-backward asymmetry in these modes could also be used to constrain NP [\[48\]](#), but [158](#)
there is no experimental information yet. [158](#)

4. $K^+ \rightarrow \pi^+ \mu^+ \mu^-$ [159](#)

Within the SM, this decay is also dominated by LD contributions that arise from an [160](#)
intermediate-photon state. The LD contributions to these modes are parameterized by the [160](#)
low-energy constants a_+ and b_+ which are themselves extracted from the measurements [\[53\]](#): [160](#)

$$\begin{aligned} \mathcal{B}_{\text{LD}}^e &= (0.15 - 3.31a_+ - 0.90b_+ + 60.51a_+^2 + 16.36a_+ b_+ + 1.77b_+^2) \times 10^{-8}, \\ \mathcal{B}_{\text{LD}}^\mu &= (1.19 - 19.97a_+ - 6.56b_+ + 120.16a_+^2 + 69.42a_+ b_+ + 10.59b_+^2) \times 10^{-9}. \end{aligned} \quad (40) \quad \text{161}$$

The values of a_+ and b_+ obtained from experiment for the electron mode [\[56\]](#) are [162](#)

$$a_+ = -0.578 \pm 0.016, \quad b_+ = -0.779 \pm 0.066 \quad (41) \quad \text{163}$$

and for the muon mode [57] 164

$$a_+ = -0.575 \pm 0.013, \quad b_+ = -0.722 \pm 0.043. \quad (42) \quad 165$$

We add possible contributions from NP to the branching ratio resulting, for the muon case, in 166

$$\begin{aligned} 10^8 \mathcal{B}(K^+ \rightarrow \pi^+ \mu^+ \mu^-) = & \mathcal{B}_{\text{LD}}^\mu + 9.66 (\lambda_t C_{7+}) + 34 (\lambda_t C_{9+}) + 17.6 (\lambda_t C_{7+})(\lambda_t C_{9+}) \\ & - 48.4 (\lambda_t C_{10+})(\lambda_t C_{P+} \text{ GeV}) + 2.5 (\lambda_t C_{7+})^2 + 31 (\lambda_t C_{9+})^2 \\ & + 74.3 (\lambda_t C_{10+})^2 + 9.46 (\lambda_t C_{P+} \text{ GeV})^2 + 4.34 (\lambda_t C_{S+} \text{ GeV})^2. \end{aligned} \quad (43) \quad 167$$

This has been partially considered in Ref. [40], which provides an expression that includes only 168 the term C_{9+}^2 with a numerical coefficient approximately twice as large as ours.¹¹ 168

A forward-backward asymmetry can be defined for this mode in terms of the angle $\theta_{K\mu}$ between 169 the charged-kaon and muon three-momenta in the dilepton center-of-mass frame [58]. 169

$$A_{\text{FB}, K^+} = \frac{\mathcal{N}(\cos \theta_{K\mu} > 0) - \mathcal{N}(\cos \theta_{K\mu} < 0)}{\mathcal{N}(\cos \theta_{K\mu} > 0) + \mathcal{N}(\cos \theta_{K\mu} < 0)}. \quad (44) \quad 186 \quad 149$$

In terms of the NP coefficients, the asymmetry is given by¹² 171

$$A_{\text{FB}, K^+} = [0.51 + 0.844 (\lambda_t C_{9+}) + 0.24 (\lambda_t C_{7+})] (\lambda_t C_{S+} \text{ GeV}). \quad (45) \quad 153 \quad 155$$

The latest measurements of these observables produced $\mathcal{B}(K^+ \rightarrow \pi^+ \mu^+ \mu^-) = (9.17 \pm 0.08) \times 10^{-8}$ 173 and $A_{\text{FB}, K^+} = (0.0 \pm 0.7) \times 10^{-2}$ [57]. 173

Constraints on NP must rely on comparisons between the muon and electron modes and arise 174 from LFU violation (LFUV). One possibility is to take the difference between the branching 174 fraction $\mathcal{B}(K^+ \rightarrow \pi^+ \mu^+ \mu^-)$ evaluated with a_+ and b_+ extracted from the muon mode, Eq. (41), 174 and with a_+ and b_+ from the electron mode, Eq. (42). 174

$$\Delta \mathcal{B}(K^+ \rightarrow \pi^+ \mu^+ \mu^-) = (-4 \pm 5) \times 10^{-9}, \quad (46) \quad 190$$

and to attribute this difference to the NP terms in Eq. (43). 176

A second possibility is to compare the parameter a_+ as extracted from the muon and electron 177 modes [49, 59]. 177

$$a_+^{\mu\mu} - a_+^{ee} = -\sqrt{2} [V_{td} V_{ts}^* (C_{9+}^{\mu\mu} - C_{9+}^{ee})]. \quad (47) \quad 190$$

With the current values of $a_+^{\mu\mu, ee}$ [56, 57], this translates into 179

$$a_+^{\mu\mu} - a_+^{ee} = 0.003 \pm 0.021. \quad (48) \quad 189 \quad 186$$

¹¹ This factor can be traced to an incorrect $\sqrt{2}$ in the form factor in their Eq. (4.16). 168

¹² Here we differ from [40] in that we normalize the forward-backward asymmetry to a fixed rate, the current 171 experimental value $\mathcal{B}(K^+ \rightarrow \pi^+ \mu^+ \mu^-) = (9.17 \pm 0.14) \times 10^{-8}$ [17]. 171

VII. ORGANIZING THE CONSTRAINTS 189 185 195

There are ten distinct WCs to describe NP in modes with muons and ten more in modes with electrons if we allow LFUV. Fortunately, as Table VI indicates, many of the modes depend only on one or two WCs, simplifying the numerical study. 182

A direct constraint on $C_{7,7'}$ can be obtained in principle from radiative hyperon and kaon decays [20, 44, 60]. However, our method to estimate the LD contributions to hyperon decay involves using the a and b parameters obtained from experiment, entailing that these could be contaminated by any NP of this form. In principle, a more detailed study of all radiative hyperon modes could be used to isolate any NP here, but we will not pursue it in this paper. Instead, we rely on the constraints obtained from radiative kaon modes by Ref. [44], as listed in Table VII. 185

From Eq. (28) and Tables II-III, one can infer that NP scenarios with $C_{7,7',9,9',10,10'} \sim 10^4$ and $C_{P,P',S,S'} \sim 10^5 \text{ GeV}^{-1}$ would be necessary to affect the $\Sigma^+ \rightarrow p\mu^+\mu^-$ rate at a level that could be observable over the LD contributions. Since this is significantly larger than the bounds placed by kaon physics, we will first impose the kaon restrictions and then use $\Sigma^+ \rightarrow p\mu^+\mu^-$ to constrain the directions to which the kaons are blind. We will not delve into specific ultraviolet completions in this paper, but simply note that WCs of this order would be consistent with dimensional analysis in models without the CKM suppression λ_t that occurs in the SM and that was rather arbitrarily introduced by the notation of Eq. (25). In Table VI we summarize the WCs that can introduce NP into the different kaon observables discussed thus far. 186

The observables in Table VI are restricted numerically by the 90% confidence-level (CL) bounds (ranges) [17] shown in Table VII, which also displays the corresponding limits for WCs for the cases in which only one of them is constrained. In Eq. (32) we notice that $K_L \rightarrow \mu^+\mu^-$ restrains a combination of C_{10-} and C_{P-} , which we dub C_{KL} , 187

$$C_{KL} = C_{10-} + \frac{m_{K_0}^2 m_s}{2m_\mu(m_d + m_s)} C_{P-} \simeq C_{10-} + 1.17 \text{ GeV } C_{P-}. \quad (49) \quad 202$$

Observable	WC—linear	WC—quadratic
$\mathcal{B}(K_L \rightarrow \mu^+\mu^-)$	C_{10-}, C_{P-}	C_{10-}, C_{P-}
$\mathcal{B}(K_S \rightarrow \mu^+\mu^-)$	C_{S-}	C_{S-}
$\mathcal{B}(K_L \rightarrow \pi^0\mu^+\mu^-)$	C_{S+}	C_{S+}
$\mathcal{B}(K_L \rightarrow \pi^0e^+e^-)$	C_{S+}	C_{S+}
$a_S^{\mu\mu} - a_S^{ee}$	C_{9+}	—
$a_+^{\mu\mu} - a_+^{ee}$	C_{9+}	—
A_{FB,K^+}	C_{S+}	C_{7+}, C_{9+}, C_{S+}
$\Delta\mathcal{B}(K^+ \rightarrow \pi^+\mu^+\mu^-)$	C_{7+}, C_{9+}	$C_{7+}, C_{9+}, C_{10+}, C_{S+}, C_{P+}$
$\mathcal{B}(\Sigma^+ \rightarrow p\mu^+\mu^-)$	$C_{7\pm}, C_{9\pm}$	$C_{9\pm}, C_{10\pm}, C_{S\pm}, C_{P\pm}$

TABLE VI. Wilson coefficients that affect the different kaon and hyperon observables under our scenario of CP -conserving NP. 183

Observable	90% CL range	constraint on WC		
$\mathcal{B}(K_L \rightarrow \mu^+ \mu^-)$ [17]	$(6.66, 7.02) \times 10^{-9}$	$-6.4 \leq C_{KL} \leq -4.7$ or $-1 \leq C_{KL} \leq 0.73$		
$\mathcal{B}(K_S \rightarrow \mu^+ \mu^-)$ [61]	$< 2.1 \times 10^{-10}$	$ C_{S-} < 40 \text{ GeV}^{-1}$		
$\mathcal{B}(K_L \rightarrow \pi^0 \mu^+ \mu^-)$ [62]	$< 3.8 \times 10^{-10}$	$ C_{S+} < 124 \text{ GeV}^{-1}$	190	107
$\mathcal{B}(K_L \rightarrow \pi^0 e^+ e^-)$ [63]	$< 2.8 \times 10^{-10}$	$ C_{S+} < 52 \text{ GeV}^{-1}$		47
$a_S^{\mu\mu} - a_S^{ee}$	$(-0.3, 1.3)$	$-603 < C_{9+} < 2611$		
$ a_{+}^{\mu\mu} - a_{+}^{ee} $	< 0.035	$ C_{9+} < 70$	190	190
processes	result from [44]	constraint on WC		
$K \rightarrow \pi\pi\gamma$ [44]	$ C_{\gamma}^- \lesssim 0.1 G_F m_K$	$ C_{7-} < 278$		
$K \rightarrow \gamma\gamma$ [44]	$ C_{\gamma}^{\pm} \lesssim 0.3 G_F m_K$	$ C_{7\pm} < 833$	190	186
				203

TABLE VII. The 90% CL ranges used for the different modes along with the restrictions they impose on WCs in cases in which only one WC enters the observable. $C_{KL} \equiv C_{10-} + 1.17 \text{ GeV } C_{P-}$ is the combination constrained by $K_L \rightarrow \mu^+ \mu^-$. The bounds in the last two rows are taken from Ref. [44] and are not 90% CL.

Interestingly, this is the same combination that appears in the $\Sigma^+ \rightarrow p\mu^+\mu^-$ form-factor \tilde{K}
 in Eq. (27). However, the hyperon mode also depends on C_{10-} through \tilde{F} in Eq. (26). The last
 two rows in Table VII exhibit bounds taken directly from Ref. [44].

After employing all the single parameter bounds from Table VII, we are left with the following constraints: 193

$$\begin{aligned} -1.2 \leq 10^8 \Delta\mathcal{B}(K^+ \rightarrow \pi^+ \mu^+ \mu^-) &\leq 0.4, \\ |A_{\text{FB}, K^+}(K^+ \rightarrow \pi^+ \mu^+ \mu^-)| &\leq 0.12, \\ 0.26 \leq 10^8 \mathcal{B}(\Sigma^+ \rightarrow p \mu^+ \mu^-) &\leq 5.2. \end{aligned}$$

Because the restriction from $K_L \rightarrow \mu^+ \mu^-$ is found to be much stronger than that from the Σ^+ decay, we present the results for C_{10-} and C_{P-} in terms of C_{KL} and its orthogonal counterpart on the $C_{10-} - C_{P-}$ plane, namely $C_\Sigma \equiv C_{10-} - 0.85 \text{ GeV } C_{P-}$. The allowed C_{KL} range is quoted in Table VII.

Imposing all the constraints simultaneously leads to allowed regions in C_{10+} - C_{P+} and C_Σ - C_{9-} planes that differ by an order of magnitude. We therefore display them separately in Fig. 6. The C_{10+} - C_{P+} region is dominantly constrained by $\Delta\mathcal{B}(K^+ \rightarrow \pi^+ \mu^+ \mu^-)$, whereas $\mathcal{B}(\Sigma^+ \rightarrow p \mu^+ \mu^-)$ restricts the parameters C_Σ and C_{9-} . For the latter, each of the four SM LD solutions leads to slightly different constraints, as illustrated on the right panel of Fig. 6 for the relativistic solutions. The figure shows two-dimensional projections of the full parameter space, but the numerical scan requires all parameters to satisfy all the constraints in Table VII and Eq. (50). | 196

The most important NP contribution to $\mathcal{B}(\Sigma^+ \rightarrow p\mu^+\mu^-)$ enters via C_{9-} , as suggested by the numerical entries in Table II. The allowed range of C_{9-} corresponding to each of the four relativistic solutions is exhibited on the left panel of Fig. 7. Its right panel displays the correlation between the integrated forward-backward asymmetry and the branching fraction for each of the four solutions. 198

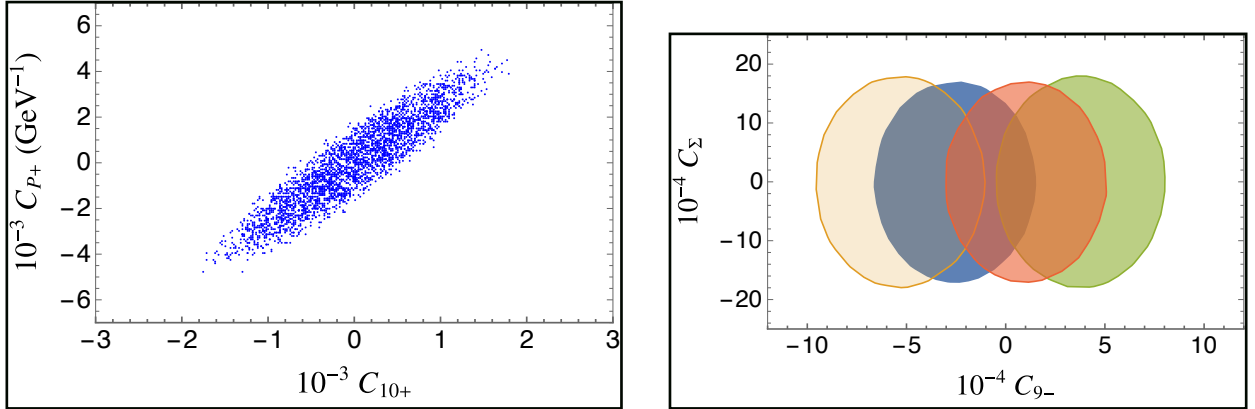


FIG. 6. Left panel: allowed C_{10+} - C_{P+} parameter space, mostly restricted by $\Delta\mathcal{B}(K^+ \rightarrow \pi^+\mu^+\mu^-)$.
 Right panel: allowed C_Σ - C_{9-} parameter space, restricted by the LHCb measurement of $\mathcal{B}(\Sigma^+ \rightarrow p\mu^+\mu^-)$. The four relativistic SM LD solutions lead to different allowed regions distinguished by the different colors (blue, yellow, green, red).
197
197
197
197

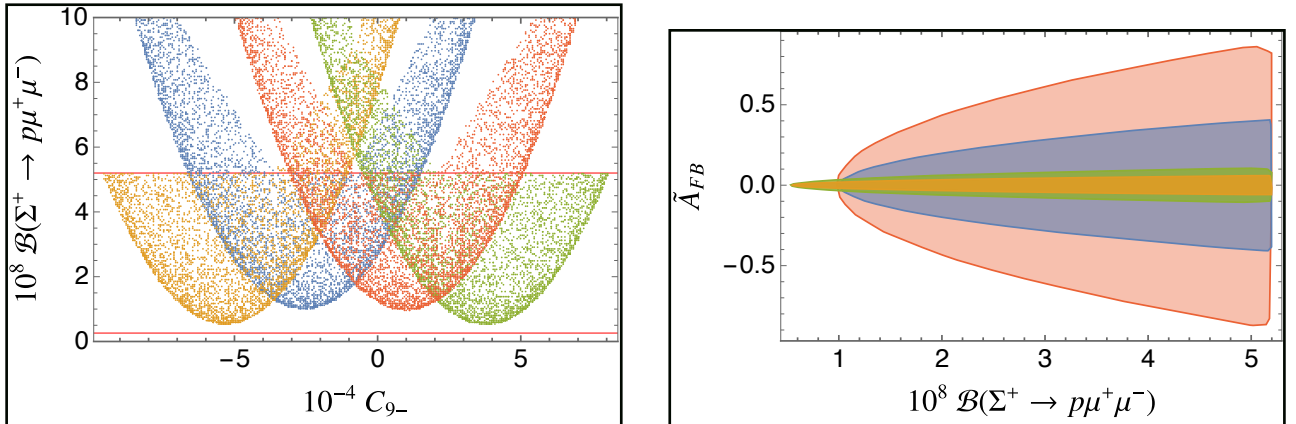


FIG. 7. Left panel: the $\Sigma^+ \rightarrow p\mu^+\mu^-$ branching fraction as a function of C_{9-} for each of the four relativistic SM LD solutions (blue, yellow, green, red). Right panel: the corresponding correlation between the branching fraction and the integrated muon forward-backward asymmetry, \tilde{A}_{FB} , in this decay mode.
199
199
199
199

The resulting integrated muon forward-backward asymmetry \tilde{A}_{FB} for $\Sigma^+ \rightarrow p\mu^+\mu^-$ across the parameter space that survives all the constraints is also most sensitive to C_{10-} , as can be inferred from Table IV. We show this in the right panel of Fig. 8 for the four relativistic SM LD solutions. The left panel exhibits the correlation between the asymmetry and C_{9-} , where the variation with C_{9-} is due to the changing rate. Although Table IV suggests that the asymmetry would be equally sensitive to C_{10+} , this is not observed in the plots because the allowed range of this parameter is considerably smaller.
200
200
200
200
200
200
200
200

It is important to note that the definition we used for \tilde{A}_{FB} allows for NP in the numerator, but is normalized to the SM rate for each of the four solutions. When the contributions of NP are large this can lead to some misleadingly large anomalies seen in Fig. 8. If we replace the
203
203
203

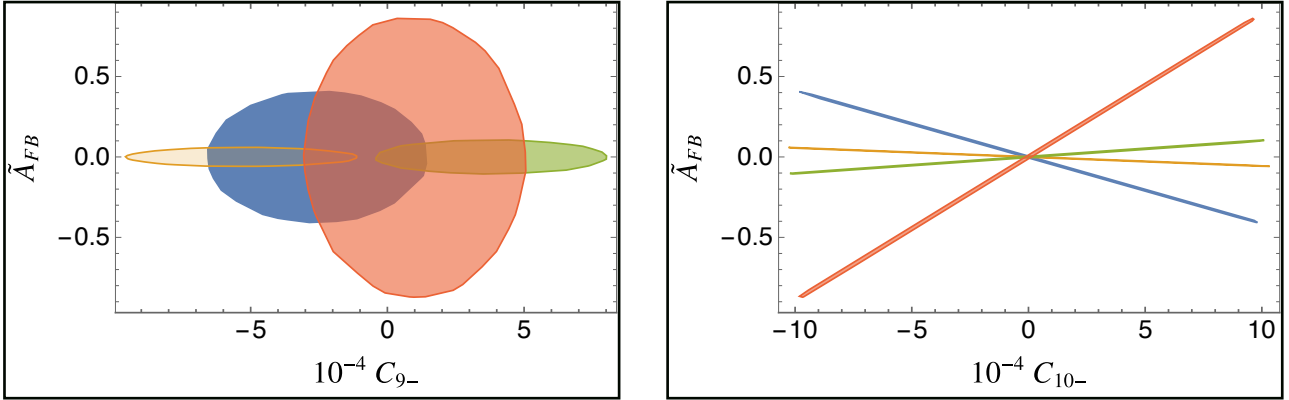


FIG. 8. The region representing the values of \tilde{A}_{FB} over the allowed range of C_{9-} (left panel) and C_{10-} (right panel) for each of the four relativistic SM LD solutions (blue, yellow, green, red). [199, 201]

denominator of the forward-backward asymmetry with the rate including NP contributions, the anomaly changes to what is exhibited in Fig. 9. [203]

VIII. SUMMARY AND CONCLUSIONS [203 189 213]

We have revisited all aspects of the calculation of the rate and muon forward-backward asymmetry for the mode $\Sigma^+ \rightarrow p\mu^+\mu^-$. This was motivated by the expected more precise measurement by LHCb as well as recent progress in related modes by BESIII. [205]

Within the SM, we corrected a long-standing issue with the short-distance contribution but found that it is still negligible with respect to the long-distance contribution. For the latter, we updated the existing experimental input which reduced the uncertainty in the predictions that is attributable to experimental error. The fourfold ambiguity in the prediction remains, but we proposed several ways to address this issue from the experimental side. With the new numbers, the estimate for hadronic error obtained by interpolating the results from leading-order relativistic baryon χ PT and from its heavy-baryon formulation is also diminished, to the extent that the four separate solutions remain separate throughout the range. [206]

We then discussed possible constraints on new physics in a model-independent manner through a general low-energy effective Hamiltonian for $s \rightarrow d\ell^+\ell^-$ processes. We considered the restrictions that can be placed on the different Wilson coefficients from the existing measurements of rare kaon decays and emphasized the usefulness of the hyperon mode in probing the directions in parameter space to which the kaons are blind. Aspects of this study exist in the literature, but this is the first such comprehensive study. Ref. [40], for example, has done a partial study of the effects of NP on the hyperon mode and the restraints from kaons. Their NP analysis of the hyperons does not contain all the possible WCs, missing in particular the interference between SM and NP in the rate which provides the most stringent constraint on C_{9-} . Within the kaon modes, we introduced a new observable to constrain NP based on the $K^+ \rightarrow \pi^+\ell^+\ell^-$ rates. [207]

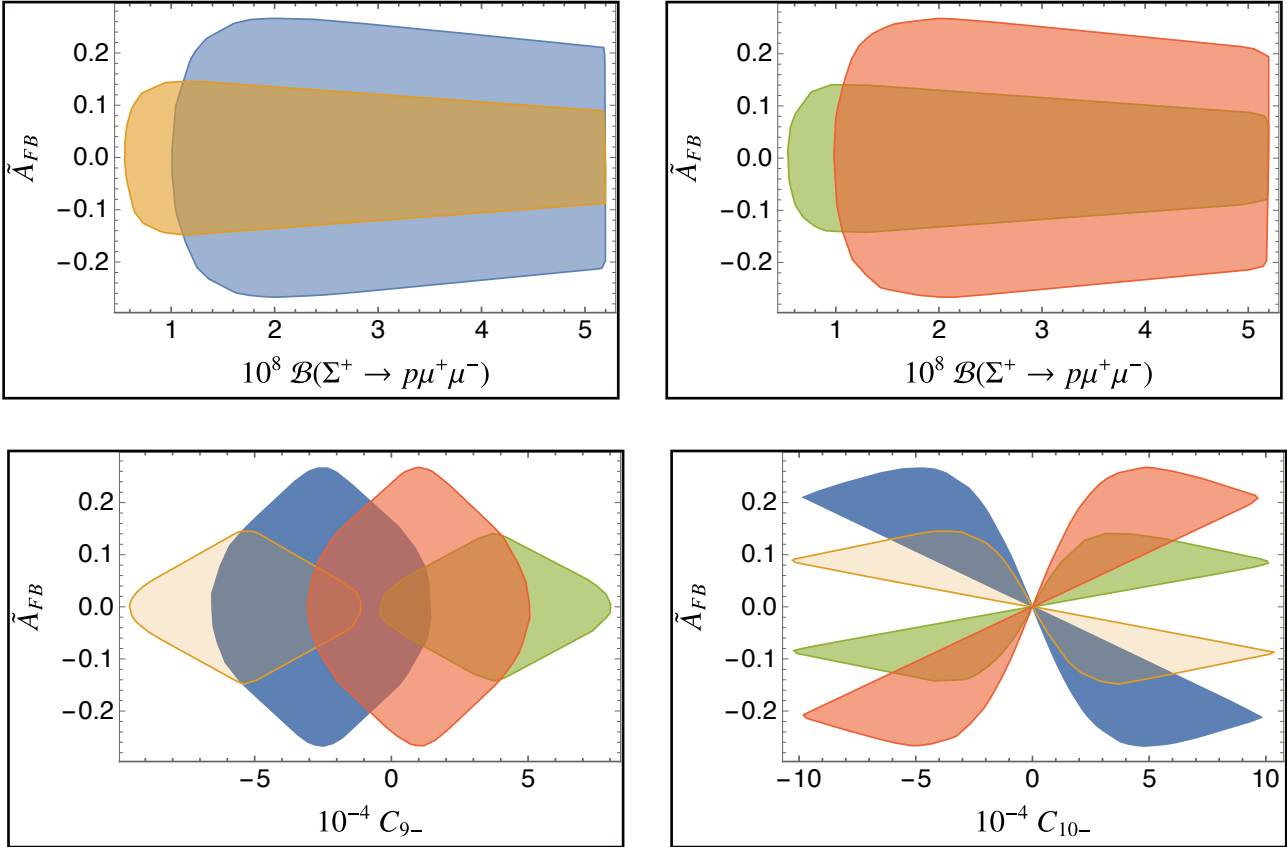


FIG. 9. Upper panels: correlation between the $\Sigma^+ \rightarrow p\mu^+\mu^-$ branching fraction and integrated muon forward-backward asymmetry, \tilde{A}_{FB} , when new physics is included in the rate normalizing the latter. Two solutions are plotted on the left panel and two on the right panel, as they overlap. Lower panels: the region representing the values of \tilde{A}_{FB} over the allowed range of C_{9-} (left panel) and C_{10-} (right panel) for each of the four relativistic SM LD solutions (blue, yellow, green, red) when new physics contributions are included in the rate normalizing the forward-backward asymmetry.

ACKNOWLEDGMENTS

We thank Cong Geng and Hong-Fei Shen for experimental information. The work of A.R. and G.V. was supported in part by an Australian Research Council Discovery Project. We are grateful to F. Mahmoudi for her help with SuperIso, which included providing us with her private code for some of the kaon modes discussed in this paper. The work of J.T. was supported in part by the National Key R&D Program of China under Contract No. 2023YFA1606000 and the National Natural Science Foundation of China (NSFC) under Contract No. 11935018. He would like to thank Hai-Bo Li and the Institute of High Energy Physics, Chinese Academy of Sciences, for kind hospitality and support during the preparation of this paper.

-
- [1] R. Aaij *et al.* (LHCb), Evidence for the rare decay $\Sigma^+ \rightarrow p\mu^+\mu^-$, *Phys. Rev. Lett.* **120**, 221803 (2018), arXiv:1712.08606 [hep-ex].
- [2] H.-B. Li, Prospects for rare and forbidden hyperon decays at BESIII, *Front. Phys. (Beijing)* **12**, 121301 (2017), [Erratum: *Front.Phys.(Beijing)* 14, 64001 (2019)], arXiv:1612.01775 [hep-ex].
- [3] A. A. Alves Junior *et al.*, Prospects for measurements with strange hadrons at LHCb, *JHEP* **05**, 048, arXiv:1808.03477 [hep-ex]. 211 215
[212 213]
- [4] R. Aaij *et al.* (LHCb), Physics case for an LHCb Upgrade II - Opportunities in flavour physics, and beyond, in the HL-LHC era, (2018), arXiv:1808.08865 [hep-ex].
- [5] A. Cerri *et al.*, Report from Working Group 4: Opportunities in Flavour Physics at the HL-LHC and HE-LHC, *CERN Yellow Rep. Monogr.* **7**, 867 (2019), arXiv:1812.07638 [hep-ph]. 213 214
[213 214]
- [6] E. Goudzovski *et al.*, New physics searches at kaon and hyperon factories, *Rept. Prog. Phys.* **86**, 016201 (2023), arXiv:2201.07805 [hep-ph]. 215 63
[203 209 216]
- [7] G. Anzivino *et al.*, Workshop summary – Kaons@CERN 2023, in *Kaons@CERN 2023* (2023) 216
arXiv:2311.02923 [hep-ph]. 216
- [8] X.-G. He, J. Tandean, and G. Valencia, The decay $\Sigma^+ \rightarrow p\ell^+\ell^-$ within the standard model, *Phys. Rev. D* **72**, 074003 (2005), arXiv:hep-ph/0506067. 221 220
- [9] M. A. Shifman, A. I. Vainshtein, and V. I. Zakharov, On the Weak Radiative Decays (Effects of Strong Interactions at Short Distances), *Phys. Rev. D* **18**, 2583 (1978), [Erratum: *Phys.Rev.D* 19, 2815 (1979)].
- [10] G. Buchalla, A. J. Buras, and M. E. Lautenbacher, Weak decays beyond leading logarithms, *Rev. Mod. Phys.* **68**, 1125 (1996), arXiv:hep-ph/9512380.
- [11] M. Ablikim *et al.* (BESIII), Precision Measurement of the Decay $\Sigma^+ \rightarrow p\gamma$ in the Process $J/\psi \rightarrow \Sigma^+\Sigma^-$, *Phys. Rev. Lett.* **130**, 211901 (2023), arXiv:2302.13568 [hep-ex].
- [12] M. Ablikim *et al.* (BESIII), Σ^+ and $\bar{\Sigma}^-$ Polarization in the J/ψ and $\psi(3686)$ Decays, *Phys. Rev. Lett.* **125**, 052004 (2020), arXiv:2004.07701 [hep-ex].
- [13] M. Ablikim *et al.* (BESIII), Test of CP Symmetry in Hyperon to Neutron Decays, *Phys. Rev. Lett.* **131**, 191802 (2023), arXiv:2304.14655 [hep-ex].
- [14] T. Inami and C. S. Lim, Effects of Superheavy Quarks and Leptons in Low-Energy Weak Processes $K_L \rightarrow \mu\bar{\mu}$, $K^+ \rightarrow \pi^+\nu\bar{\nu}$ and $K^0 \leftrightarrow \bar{K}^0$, *Prog. Theor. Phys.* **65**, 297 (1981), [Erratum: *Prog.Theor.Phys.* 65, 1772 (1981)].
- [15] J. Tandean, Rare hyperon decays with missing energy, *JHEP* **04**, 104, arXiv:1901.10447 [hep-ph].
- [16] N. Cabibbo, E. C. Swallow, and R. Winston, Semileptonic hyperon decays, *Ann. Rev. Nucl. Part. Sci.* **53**, 39 (2003), arXiv:hep-ph/0307298.
- [17] R. L. Workman and Others (Particle Data Group), Review of Particle Physics, *PTEP* **2022**, 083C01 44 246
[2022]. 47 210 211
- [18] S. Neshatpour and F. Mahmoudi, Flavour Physics Phenomenology with SuperIso, *PoS Comp. Tools2021*, 010 (2022), arXiv:2207.04956 [hep-ph].
- [19] M. Nielsen, L. A. Barreiro, C. O. Escobar, and R. Rosenfeld, A QCD sum rule approach to the $s \rightarrow d\gamma$ contribution to the $\Omega^- \rightarrow \Xi^-\gamma$ radiative decay, *Phys. Rev. D* **53**, 3620 (1996), arXiv:hep-ph/9509297.
- [20] J. Tandean, New physics and short distance $s \rightarrow d\gamma$ transition in $\Omega^- \rightarrow \Xi^-\gamma$ decay, *Phys. Rev. D* **61**, 114022 (2000), arXiv:hep-ph/9912497.
- [21] J. F. Donoghue, E. Golowich, and B. R. Holstein, *Dynamics of the Standard Model: Second edition* 211 249
[Cambridge University Press, 2022]. 230 107 63

- [22] G. Ang *et al.*, Radiative Σ^\pm decays and search for neutral currents, *Z. Phys.* **228**, 151 (1969).
- [23] H. Park *et al.* (HyperCP), Evidence for the Decay $\Sigma^+ \rightarrow p\mu^+\mu^-$, *Phys. Rev. Lett.* **94**, 021801 (2005), arXiv:hep-ex/0501014.
- [24] R. E. Behrends, Photon Decay of Hyperons, *Phys. Rev.* **111**, 1691 (1958).
- [25] I. V. Lyagin and E. K. Ginzburg, On $\Sigma^+ \rightarrow pe^+e^-$ and $\Sigma^+ \rightarrow p\mu^+\mu^-$ Decays, *Sov. Phys. JETP* **14**, 653 (1962).
- [26] L. Bergstrom, R. Safadi, and P. Singer, Phenomenology of $\Sigma^+ \rightarrow p\ell^+\ell^-$ and the structure of the weak non-leptonic Hamiltonian, *Z. Phys. C* **37**, 281 (1988).
- [27] L. K. Gershwin, M. Alston-Garnjost, R. O. Bangerter, A. Barbaro-Galtieri, T. S. Mast, F. T. Solmitz, and R. D. Tripp, Asymmetry parameter and branching ratio of $\Sigma^+ \rightarrow p\gamma$, *Phys. Rev.* **188**, 2077 (1969).
- [28] A. Manz, S. Reucroft, R. Settles, G. Wolf, J. Marraffino, C. Roos, J. Waters, and M. Webster, A new measurement of $\Sigma^+ \rightarrow p\gamma$ decay properties, *Phys. Lett. B* **96**, 217 (1980).
- [29] M. Kobayashi, J. Haba, T. Homma, H. Kawai, K. Miyake, T. S. Nakamura, N. Sasao, and Y. Sugimoto, New measurement of the asymmetry parameter for the $\Sigma^+ \rightarrow p\gamma$ decay, *Phys. Rev. Lett.* **59**, 868 (1987).
- [30] M. Foucher *et al.* (E761), Measurement of the asymmetry parameter in the hyperon radiative decay $\Sigma^+ \rightarrow p\gamma$, *Phys. Rev. Lett.* **68**, 3004 (1992).
- [31] R. Aaij *et al.* (LHCb), Measurement of the photon polarization in $\Lambda_b^0 \rightarrow \Lambda\gamma$ decays, *Phys. Rev. D* **105**, L051104 (2022), arXiv:2111.10194 [hep-ex].
- [32] R. O. Bangerter, *Nonleptonic decay of Sigma hyperons*, Ph.D. thesis, Calif. U. Berkeley (1969).
- [33] F. Harris, O. E. Overseth, L. Pondrom, and E. Dettmann, Proton Polarization in $\Sigma^+ \rightarrow p\pi^0$, *Phys. Rev. Lett.* **24**, 165 (1970).
- [34] E. H. Bellamy *et al.*, Polarisation in the reaction $\pi^+p \rightarrow K^+\Sigma^+$ at 1.11 GeV/c, *Phys. Lett. B* **39**, 299 (1972).
- [35] N. H. Lipman *et al.*, A test of the $\Delta I = 1/2$ rule and the Lee-Sugawara relation in the decay $\Sigma^+ \rightarrow p\pi^0$, *Phys. Lett. B* **43**, 89 (1973).
- [36] F. Erben, V. Gülpers, M. T. Hansen, R. Hodgson, and A. Portelli, Prospects for a lattice calculation of the rare decay $\Sigma^+ \rightarrow p\ell^+\ell^-$, *JHEP* **04**, 108, arXiv:2209.15460 [hep-lat].
- [37] F. Erben, V. Gülpers, M. T. Hansen, R. Hodgson, and A. Portelli, Progress on the exploratory calculation of the rare Hyperon decay $\Sigma^+ \rightarrow p\ell^+\ell^-$, *PoS LATTICE2022*, 315 (2023), arXiv:2212.09595 [hep-lat].
- [38] X.-G. He, J. Tandean, and G. Valencia, Decay rate and asymmetries of $\Sigma^+ \rightarrow p\mu^+\mu^-$, *JHEP* **10**, 040, arXiv:1806.08350 [hep-ph].
- [39] R. Aaij *et al.* (LHCb), Differential branching fraction and angular analysis of $\Lambda_b^0 \rightarrow \Lambda\mu^+\mu^-$ decays, *JHEP* **06**, 115, [Erratum: JHEP 09, 145 (2018)], arXiv:1503.07138 [hep-ex].
- [40] L.-S. Geng, J. M. Camalich, and R.-X. Shi, New physics in $s \rightarrow d$ semileptonic transitions: rare hyperon vs. kaon decays, *JHEP* **02**, 178, arXiv:2112.11979 [hep-ph].
- [41] G. Isidori, C. Smith, and R. Unterdorfer, The rare decay $K_L \rightarrow \pi^0\mu^+\mu^-$ within the SM, *Eur. Phys. J. C* **36**, 57 (2004), arXiv:hep-ph/0404127.
- [42] F. Mahmoudi, SuperIso v3.0, flavor physics observables calculations: Extension to NMSSM, *Comput. Phys. Commun.* **180**, 1718 (2009).
- [43] S. Neshatpour and F. Mahmoudi, Flavour Physics with SuperIso, *PoS TOOLS2020*, 036 (2021), arXiv:2105.03428 [hep-ph].
- [44] P. Mertens and C. Smith, The $s \rightarrow d\gamma$ decay in and beyond the Standard Model, *JHEP* **08**, 069, arXiv:1103.5992 [hep-ph].

44 246
241 107 63

- [45] V. Chobanova, G. D'Ambrosio, T. Kitahara, M. Lucio Martinez, D. Martinez Santos, I. S. Fernandez, and K. Yamamoto, Probing SUSY effects in $K_S^0 \rightarrow \mu^+ \mu^-$, *JHEP* **05**, 024, arXiv:1711.11030 [hep-ph]. 254
- [46] M. Gorbahn and U. Haisch, Charm Quark Contribution to $K_L \rightarrow \mu^+ \mu^-$ at Next-to-Next-to-Leading Order, *Phys. Rev. Lett.* **97**, 122002 (2006), arXiv:hep-ph/0605203. 254
- [47] G. Buchalla, G. D'Ambrosio, and G. Isidori, Extracting short distance physics from $K_{L,S} \rightarrow \pi^0 e^+ e^-$ decays, *Nucl. Phys. B* **672**, 387 (2003), arXiv:hep-ph/0308008.
- [48] F. Mescia, C. Smith, and S. Trine, $K_L \rightarrow \pi^0 e^+ e^-$ and $K_L \rightarrow \pi^0 \mu^+ \mu^-$: a binary star on the stage of flavor physics, *JHEP* **08**, 088, arXiv:hep-ph/0606081.
- [49] G. D'Ambrosio, A. M. Iyer, F. Mahmoudi, and S. Neshatpour, Anatomy of kaon decays and prospects for lepton flavour universality violation, *JHEP* **09**, 148, arXiv:2206.14748 [hep-ph].
- [50] G. Ecker, A. Pich, and E. de Rafael, $K \rightarrow \pi \ell^+ \ell^-$ decays in the effective chiral lagrangian of the standard model, *Nucl. Phys. B* **291**, 692 (1987).
- [51] G. D'Ambrosio, G. Ecker, G. Isidori, and J. Portoles, The decays $K \rightarrow \pi \ell^+ \ell^-$ beyond leading order in the chiral expansion, *JHEP* **08**, 004, arXiv:hep-ph/9808289.
- [52] G. D'Ambrosio, D. Greynat, and M. Knecht, On the amplitudes for the CP-conserving $K^\pm(K_S) \rightarrow \pi^\pm(\pi^0)\ell^+ \ell^-$ rare decay modes, *JHEP* **02**, 049, arXiv:1812.00735 [hep-ph].
- [53] V. Cirigliano, G. Ecker, H. Neufeld, A. Pich, and J. Portoles, Kaon Decays in the Standard Model, *Rev. Mod. Phys.* **84**, 399 (2012), arXiv:1107.6001 [hep-ph].
- [54] J. R. Batley *et al.* (NA48/1), Observation of the rare decay $K_S \rightarrow \pi^0 e^+ e^-$, *Phys. Lett. B* **576**, 43 (2003), arXiv:hep-ex/0309075 [hep-ex].
- [55] J. R. Batley *et al.* (NA48/1), Observation of the rare decay $K_S \rightarrow \pi^0 \mu^+ \mu^-$, *Phys. Lett. B* **599**, 197 (2004), arXiv:hep-ex/0409011 [hep-ex].
- [56] J. R. Batley *et al.* (NA48/2), Precise measurement of the $K^\pm \rightarrow \pi^\pm e^+ e^-$ decay, *Phys. Lett. B* **677**, 246 (2009), arXiv:0903.3130 [hep-ex].
- [57] E. Cortina Gil *et al.* (NA62), A measurement of the $K^+ \rightarrow \pi^+ \mu^+ \mu^-$ decay, *JHEP* **11**, 011, [Addendum: *JHEP* 06, 040 (2023)], arXiv:2209.05076 [hep-ex].
- [58] C.-H. Chen, C. Q. Geng, and I.-L. Ho, Forward backward asymmetry in $K^+ \rightarrow \pi^+ l^+ l^-$, *Phys. Rev. D* **67**, 074029 (2003), arXiv:hep-ph/0302207. 44 246
- [59] A. Crivellin, G. D'Ambrosio, M. Hoferichter, and L. C. Tunstall, Violation of lepton flavor and lepton flavor universality in rare kaon decays, *Phys. Rev. D* **93**, 074038 (2016), arXiv:1601.009701.166 [hep-ph]. 268
- [60] X.-G. He and G. Valencia, Constraints on $s \rightarrow d\gamma$ from radiative hyperon and kaon decays, *Phys. Rev. D* **61**, 075003 (2000), arXiv:hep-ph/9908298. 270 268
- [61] R. Aaij *et al.* (LHCb), Constraints on the $K_S^0 \rightarrow \mu^+ \mu^-$ Branching Fraction, *Phys. Rev. Lett.* **125**, 231801 (2020), arXiv:2001.10354 [hep-ex].
- [62] A. Alavi-Harati *et al.* (KTeV), Search for the Decay $K_L \rightarrow \pi^0 \mu^+ \mu^-$, *Phys. Rev. Lett.* **84**, 5279 (2000), arXiv:hep-ex/0001006 [hep-ex].
- [63] A. Alavi-Harati *et al.* (KTeV), Search for the Rare Decay $K_L \rightarrow \pi^0 e^+ e^-$, *Phys. Rev. Lett.* **93**, 021805 (2004), arXiv:hep-ex/0309072 [hep-ex]. 272 271